J. Fluid Mech. (1999), *vol.* 395, *pp.* 89–124. Printed in the United Kingdom

Ocean waves and ice sheets

By N. J. BALMFORTH[1] AND R. V. CRASTER[2]

[1]Instituto di Cosmogeofisica, C. Fiume 4, 10133 Torino, Italia

[2]Department of Mathematics, Imperial College of Science, Technology and Medicine, London, SW7 2BZ, UK

(Received 4 December 1998 and in revised form 4 February 1999)

A complete analytical study is presented of the reflection and transmission of surface gravity waves incident on ice-covered ocean. The ice cover is idealized as a plate of elastic material for which flexural motions are described by the Timoshenko–Mindlin equation. A suitable non-dimensionalization extracts parameters useful for the characterization of ocean-wave and ice-sheet interactions, and for scaled laboratory studies. The scattering problem is simplified using Fourier transforms and the Wiener–Hopf technique; the solution is eventually written down in terms of some easily evaluated quadratures. An important feature of this solution is that the physical conditions at the edge of the ice sheet are explicitly built into the analysis, and power-flow theorems provide verification of the results. Asymptotic results for large and small values of the non-dimensional parameters are extracted and approximations are given for general parameter values.

1. Introduction

In the polar oceans, surface gravity waves propagate from the open ocean into ice-covered seas; these waves have been observed to travel over extensive regions in the form of flexing motions of the ice cover (Hunkins 1962; Robin 1963). Such *flexural* waves have been observed in many different types of sea ice from frazil or grease ice (Martin & Kauffman 1981; Wadhams & Holt 1991) to pack ice (Robin 1963) and even glacial ice tongues (Holdsworth 1969; Squire *et al.* 1994). The very latest measurements (Liu, Holt & Vachon 1991) are sufficiently detailed to allow quantitative comparisons with theoretical predictions and this has triggered some studies of ice-sheet and ocean-wave interactions (Squire *et al.* 1995).

There has also been recent theoretical interest in the subject in view of the possibility that incident ocean waves play the primary role in fracturing shore-fast sea ice and extensive ice floes (Fox & Squire 1994). Physical evidence for this fracturing process arises from the observation that cracks in thin floating ice sheets often appear close to the ice edge; the interpretation is that they are generated by stresses caused within the ice by transmitted ocean waves (Squire *et al.* 1995). This fracturing process is a plausible explanation for the break-up of shore-fast sea ice, but has also been suggested to lie at the heart of the calving of icebergs from ice tongues (Holdsworth & Glynn 1981).

A theory of the fracturing process contains a wealth of complicated physical ingredients, and considerable idealization is needed in any model. Previous studies have outlined one approach to the problem. The foundation of this approach is a linear scattering theory of waves incident on the ice edge, assuming the ice sheet to be a very thin, homogeneous plate of some known material. The scattering

theory provides the form of disturbances transmitted into the plate. Then, given the associated displacements of the plate, one can estimate the resulting stresses and strains in the ice sheet. It is the action of these stresses and strains that, in this vision of the phenomenon, leads to fracture. In particular, fracture occurs either as an instantaneous mechanical failure or through the more gradual process of crack propagation and fatigue. But the goal of the approach is that, once the stresses and strains are known, one can estimate the moment of fracture and subsequent break-up of the ice sheet (Squire 1984). In this study, we will also follow this recipe, and focus upon an analytical solution of the underlying scattering problem.

Historically, the study of the propagation of ocean waves in sea ice dates back to Greenhill (1887) who considered how the dispersion relation of surface gravity waves was modified by the presence of a thin elastic beam floating on the water. Rather later, Weitz & Keller (1950) and Shapiro & Simpson (1953) used a related idealization of the problem to study how waves incident on an ice-covered sea were reflected and transmitted. These authors modelled the ice sheet as a floating set of disconnected mass points; this incorporates only the physical effect of the mass loading of the ocean surface, and neglects any effects resulting from the horizontal structure of the ice cover or the interaction of adjacent ice floes.

For flexural waves in a connected ice sheet, an essential physical effect is the elasticity of the ice cover (Robin 1963). For this reason, the idealization of the ice sheet as a floating elastic plate (Greenhill's original visualization) is more popular. This model is central to the (sadly unpublished) work of Evans & Davies (1968), thesis and papers by Wadhams (1973*a*, *b*, 1986), and the much more recent series of papers by Fox & Squire (1990, 1991, 1994). These authors also tackled the transmission problem, and the study presented here closely follows the direction initiated by Evans & Davies.

Evans & Davies present a solution method based on the Wiener–Hopf technique. This method generates an explicit solution that requires the computation of the ratio of some infinite products. Those infinite products require some work to evaluate from a numerical perspective, and this feature of their solution has apparently dissuaded subsequent workers from exploiting it. The method presented by Evans & Davies is made yet more convoluted by the manner in which the physical conditions at the ice edge are incorporated into the calculation. However, as we indicate in this study, edge conditions can be included more straightforwardly, and ultimately one can compute the exact solution through some simply evaluated quadratures. These improvements make Evans & Davies's solution substantially more useful computationally.

The more recent studies of Fox & Squire are summarized in Squire *et al.* (1995) and make no attempt to extract an analytical solution. The approach taken in these works is numerically based, and involves expansions in normal modes similar to those used in waveguide theory (Mittra & Lee 1971). Though this is a versatile technique, there are complications in the current application due to the edge of the ice sheet. It is not clear how accurately the numerical, mode-matching studies deal with this aspect of the problem, and the techniques have some problems of inconsistency (Fox & Squire 1990). Moreover, the approach offers no analytical inroads into the problem.

By contrast, an exact solution has edge conditions explicitly incorporated.† Moreover, it is possible to extract simpler forms of the exact solution in certain limiting

† The detailed edge conditions have been the focus of many studies in the related field of structural acoustics where similar plate theories are often adopted (a useful introduction is given by Crighton 1988); although there are several differences we use many ideas from that theory.

cases, and to find useful approximations to the general problem. Partly for these reasons, we here expand further on the Evans & Davies study. More specifically, we give a complete discussion of the analytical solution of the scattering problem. However, we depart from Evans & Davies's analysis by deriving computationally effective tools to evaluate the exact solution, by explicitly incorporating the edge conditions, and by looking further into asymptotic and approximate solutions.

Another way in which we differ from Evans & Davies is that we consider more general models for the ice sheet. This is partly to accommodate more physics in the problem, but it also highlights the versatility of the Wiener–Hopf technique. More specifically, we use the Timoshenko–Mindlin equation (Mindlin 1951) to describe the flexing of the ice sheet. This model equation incorporates some further physical effects over the thin-plate equation used by Evans & Davies (see Junger & Feit 1986). Some aspects of the additional physics are brought out in the discussion of this paper, but at heart, the Timoshenko–Mindlin equation allows for ice sheets of greater thickness. This type of modification may therefore be needed in considering relatively thick sheets such as ice shelves and ice tongues, though Fox & Squire (1991) report some calculations suggesting that the thin-plate theory is adequate even in these problems. In fact, as we show later, the gathering together of the physical variables into various non-dimensional parameters illustrates that this result can be seen from a relatively early stage.

A second modification is to include some effects of compressibility. There are two ways that such effects could enter the problem. One is through compressive stresses in the ice sheet itself (Bates & Shapiro 1980; Liu & Mollo-Christensen 1988) and adds terms that can lead to the possibility of structural failure through buckling instability. Such stresses could be relevant if the ice sheet was under compression due to partial encirclement by land; the riding of ice plates over one another, and the formation of ice ridges suggest the existence of such stresses. Compressible effects could also enter through the fluid equations (Bates & Shapiro 1980). However, this latter effect is only important at very high wave frequencies (such as might be generated by explosions or machines; see Bates & Shapiro 1980), and is of less interest in the applications envisaged here, so we ignore it (but, in principle, compressible ocean waves could also be handled with the Wiener–Hopf methodology).

Another extension of the theory is the addition of dissipative effects (Wadhams 1986). In structural acoustics, it is typical to add dissipative effects in the plate equation by allowing for an imaginary part to the flexural rigidity (Ungar 1988). This imaginary correction provides damping within the plate and has been used to model viscoelastic coatings which reduce the amplitude of scattered waves. In fact, Squire (1984) has previously derived a complex flexural rigidity from a viscoelastic model of an ice sheet. Another inelastic effect that has been added to the plate equations is a simple form of friction (e.g. Robinson & Palmer 1990); this addition has been used by Fox & Squire (1992) to improve comparisons between theory and flexural-wave observations. Our main reasons for including dissipation are to consider wave attenuation for some simple models, and to indicate how such dissipation modifies the analysis of the scattering problem.

The various extensions of the thin-plate theory all lead to problems that can be dealt with using Wiener–Hopf techniques. We formulate the general problem in § 2. Sections 3 and 4 describe special limits and the controlling non-dimensional parameters. After an essential prelude in which we consider wave propagation (§ 5), we give the formal general solution in § 6. However, for the purposes of illustration, we consider the thin-plate model and focus on the computation of reflection and transmission coefficients

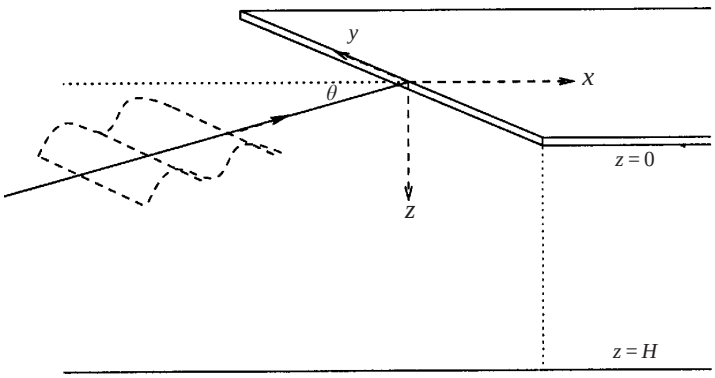

FIGURE 1. The geometry of the problem. The angle of incidence, θ, is the angle made between the wavenumber vector and the (horizontal) normal to the ice of the ice sheet.

(§§ 7 and 8). These coefficients measure the amplitudes of waves reflected from the ice edge or transmitted into the ice sheet, relative to the incident wave amplitude. Given such coefficients, one can estimate the wave amplitudes within the ice sheet and conjecture whether the sheet fractures; other uses are described by Squire *et al.* (1995). We present a summary and outline some perspectives for future work in § 9. A concise form of our results is found in table 4 which displays the formulae for the reflection and transmission coefficients, both for the full problem and for also various asymptotic limits and approximations. The Appendices contain some necessary technical details.

2. Formulation

We consider the configuration shown in figure 1, in which an open ocean adjoins a region covered with a thin, homogeneous sheet of ice. Surface gravity waves are incident on the ice-covered sea from the open ocean. If we assume these waves are irrotational, incompressible and of low enough amplitude that nonlinear terms can be neglected, then motion is described by a velocity potential of the form, $\mathrm{Re}[\hat{\phi}(x', y', z')\mathrm{e}^{-\mathrm{i}\omega t}]$, satisfying

$$\frac{\partial^2\hat{\phi}}{\partial x'^2} + \frac{\partial^2\hat{\phi}}{\partial y'^2} + \frac{\partial^2\hat{\phi}}{\partial z'^2} = 0. \tag{2.1}$$

The explicit time dependence $\mathrm{e}^{-\mathrm{i}\omega t}$ is considered understood throughout, and is henceforth suppressed.

In this study we focus on waves in a fluid of finite depth, d. The fluid lies in the region $-\infty < x', y' < \infty$, $0 < z' < d$. The ice sheet covers the fluid in the region $x' > 0$; the ocean surface for $x' < 0$ is free.

In linear theory, the boundary condition at the free surface is

$$z' = 0, \quad x' < 0 : \quad K\hat{\phi} + \hat{\phi}_{z'} = 0, \tag{2.2}$$

where $K = \omega^2/g$ is the wavenumber of surface gravity waves in open water of infinite depth, and g is the acceleration due to gravity. This free-surface condition ignores effects such as the original generation of the waves through atmospheric forcing. Instead, we input the waves directly by prescribing an incident wave field at one edge of the domain.

The fluid has finite depth, d, and we impose a no-flow condition on the ocean bed:

$$\hat{\phi}_{z'} = 0 \quad \text{on } z' = d. \tag{2.3}$$

In the limit in which the ocean depth becomes infinite, we replace this boundary condition by the requirement that $\hat{\phi} \to 0$ as $z' \to \infty$.

2.1. *The plate equation for the ice sheet*

The boundary condition for $z' = 0$ and $x' > 0$ is substantially more complicated since it models the physics associated with how the ice sheet deforms as the waves propagate through it. We cannot hope to treat this deformation exactly, and so we will follow conventional wisdom and adopt the idealization that the ice sheet acts like an elastic plate floating atop the water. The equations of motion of the elastic plate are further simplified if the sheet is thin compared to the wavelength of the incoming waves. Then we may use a 'thin plate' approximation (e.g. Junger & Feit 1986) and write down a boundary condition on $z' = 0$ and $x' > 0$ that models the dynamics of the deforming ice sheet. Conventionally, this is the thin-plate equation that includes elastic effects, but here we adopt the slightly more complicated Timoshenko–Mindlin equation (Mindlin 1951).

We further allow for a mean compressive stress in the ice sheet (Bates & Shapiro 1980; Liu & Mollo-Christensen 1988). Such a force can only be imposed parallel to the ice edge (in the y-direction; *laterally*) for the semi-infinite sheet, unless we consider some unphysical clamping force on the ice edge.

Lastly, as mentioned in the introduction, we include dissipation in the ice sheet. Because the true form of the dissipation is not known (and in reality highly complicated), it is convenient to adopt simple, yet physically plausible, models of dissipation. The two terms we include are an imaginary part in the flexural rigidity (Ungar 1988) and a simple friction term (Robinson & Palmer 1990). Whether these forms of dissipation are consistent with observations will be briefly considered later.

For our model, the dynamics of the flexing ice sheet is incorporated via the boundary condition

$$z = 0, \quad x > 0: \quad \left[(B\nabla^2 + m\omega^2 I)\left(\nabla^2 + m\omega^2 \frac{S}{B}\right) + hP\frac{\partial^2}{\partial y'^2} + \rho g - m\omega^2 - \mathrm{i}m\Pi\omega\right] \times \frac{\partial \hat{\phi}}{\partial z'} + \rho\omega^2\left(1 - S\nabla^2 - m\omega^2\frac{IS}{B}\right)\hat{\phi} = 0 \tag{2.4}$$

(see also Fox & Squire 1991). Here, ∇^2 is the horizontal Laplacian,

$$\nabla^2 \equiv \frac{\partial^2}{\partial x'^2} + \frac{\partial^2}{\partial y'^2}, \tag{2.5}$$

and the various constants are as follows. The bending stiffness (the flexural rigidity) of the plate is B, and m is the mass per unit area; ρ is the density of sea water. In more conventional notation,

$$B = [Eh^3/12(1 - \nu^2)]\mathrm{e}^{\mathrm{i}\varphi} \quad \text{and} \quad m = \rho_i h, \tag{2.6}$$

where E, is Young's modulus, h is the plate thickness, and ν and ρ_i are the Poisson ratio and mass density of the elastic material (ice) respectively. The phase, φ, of B introduces our first dissipative term, an imaginary component of the flexural rigidity.

Constants	Typical value	Source
E	6×10^9 Pa	Wadhams (1973*a*)
ν	0.3	Robin (1963)
ρ	1025 kg m^{-3}	
ρ_i	922.5 kg m^{-3}	
P	10^6 N m^{-2}	Suggested by Liu & Mollo-Christensen 1988

TABLE 1. The physical constants that appear in the scattering problem, together with typical values taken from the sources also listed.

Physical variable	Typical range of values	Characteristic value	Normalized range	Source
ω	0.1–10 rad s^{-1}	$\omega_* = 1$ rad s^{-1}	0.1–10	Lighthill (1978)
h	0.5–8.0 m	$h_* = 1$ m	0.5–8.0	Wadhams (1995)
d	10 m–∞	$d_* = 100$	0.1–∞	Evans & Davies (1968)

TABLE 2. The physical variables that appear in the scattering problem that may take a range of values depending on the setting. These are given characteristic values (denoted by the subscript $*$) and the normalized range of possible values is also listed.

Additionally,

$$I = \tfrac{1}{12}h^2 \quad \text{and} \quad S = \frac{12B}{\pi^2 Gh} \tag{2.7}$$

denote the rotary inertia and shear deformation of the plate; $G = E/2(1+\nu)$ is the shear modulus of the elastic material. The compressive stress in the y-direction is P. The second effect of damping appears through Π, the frictional damping rate (with units of inverse time), such as might occur if there were a thin, dissipative layer between the ice and water.

Values of the main physical constants appearing in these formulae are given in table 1. In table 2 we also list the ranges of possible values for ω, h and d.

2.2. *Conditions at the edge of the ice sheet*

Another important feature when dealing with elastic-plate equations is the imposition of edge conditions on the plate. Here we adopt the conditions of no external force and bending moment at the plate edge (Timoshenko & Woinowsky-Krieger 1959). These conditions, imposed at $z' = 0$ and $x' = 0^+$, can be cast in the form

$$\left(\frac{\partial^2}{\partial x'^2} + \nu\frac{\partial^2}{\partial y'^2}\right)\hat{\phi}_{z'} = 0 \tag{2.8}$$

and

$$\left[\frac{\partial^3}{\partial x'^3} + (2-\nu)\frac{\partial^3}{\partial x'\partial y'^2} + m\omega^2\frac{(S+I)}{B}\frac{\partial}{\partial x'}\right]\hat{\phi}_{z'} = 0 \tag{2.9}$$

(cf. Fox & Squire 1991).

2.3. *Non-dimensionalization*

To reduce the number of free variables, and ease the identification of limiting cases, we now non-dimensionalize the equations. To measure length, L, we adopt a unit

based on wavenumber, $L = K^{-1} \equiv g/\omega^2$, and set

$$(x, y, z) = K(x', y', z').$$

Since we deal only with linear theory there is no need to non-dimensionalize $\hat{\phi}$. However, for convenience, we scale $\hat{\phi}$ such that the incident wave amplitude at the surface is unity.

The only important ramification of the non-dimensionalization is to isolate various non-dimensional groups in the governing equations and simplify the appearance of the equations. This has the useful effect that one can quickly determine which parameters in a specific model are of importance, and which have significantly less effect.

The potential equation becomes

$$\frac{\partial^2\hat{\phi}}{\partial x^2} + \frac{\partial^2\hat{\phi}}{\partial y^2} + \frac{\partial^2\hat{\phi}}{\partial z^2} = 0, \tag{2.10}$$

subject to the boundary conditions

$$z = 0, \quad x < 0: \quad \hat{\phi} + \hat{\phi}_z = 0, \tag{2.11}$$

$$z = 0, \quad x > 0: \quad \left[\epsilon\nabla^4 + (\zeta + \sigma)\nabla^2 + p\frac{\partial^2}{\partial y^2} + \delta - 1 + \frac{\zeta\sigma}{\epsilon} - \mathrm{i}\varpi\right]\hat{\phi}_z + \delta\left(1 - \sigma\nabla^2 - \frac{\zeta\sigma}{\epsilon}\right)\hat{\phi} = 0, \tag{2.12}$$

where $\nabla^2 \equiv \partial_x^2 + \partial_y^2$, and

$$\hat{\phi}_z(x, y, H) = 0 \tag{2.13}$$

(or $\hat{\phi} \to 0$ as $z \to \infty$ for the case of infinite depth), and the edge conditions

$$\left(\frac{\partial^2}{\partial x^2} + \nu\frac{\partial^2}{\partial y^2}\right)\hat{\phi}_z(0^+, y, 0) = 0 \tag{2.14}$$

and

$$\left[\frac{\partial^3}{\partial x^3} + (2 - \nu)\frac{\partial^3}{\partial x \partial y^2} + \frac{(\zeta + \sigma)}{\epsilon}\frac{\partial}{\partial x}\right]\hat{\phi}_z(0^+, y, 0) = 0. \tag{2.15}$$

The non-dimensional groups in these equations are listed in table 3. The parameters ϵ, δ, ζ, σ and p are, respectively, measures of the ice sheet's elasticity, the degree of mass loading, the rotary inertia, the shear deformation and the compressive stress. The parameters determining the dissipation are $\mathrm{Arg}(\epsilon) \equiv \varphi$ and ϖ. The non-dimensional depth, $H = Kd$ also appears. In table 3, we list the dependence of these parameters upon the wave frequency, the ice thickness and the ocean depth.

2.4. *Isolation of the incident and scattered fields*

The final piece of the formulation of the problem is to isolate the incident wave. The incoming surface waves from $x = -\infty$ are taken to be of the form

$$\phi^{inc}(x, y, z) = \frac{\cosh\mu(z - H)}{\cosh\mu H}\exp(\mathrm{i}\gamma x + \mathrm{i}\kappa y), \tag{2.16}$$

Parameter	Definition	Dependence on normalized variables
H	$\frac{1}{g}\omega^2 d$	$10.19\frac{d}{d_*}\left(\frac{\omega}{\omega_*}\right)^2$
ϵ	$\frac{E}{12\rho_i g^4(1-\nu^2)}h^2\omega^6 e^{i\varphi}$	$10.71\left(\frac{h}{h_*}\right)^2\left(\frac{\omega}{\omega_*}\right)^6 e^{i\varphi}$
δ	$\frac{\rho g}{\rho_i}h^{-1}\omega^{-2}$	$10.9\left(\frac{h}{h_*}\right)^{-1}\left(\frac{\omega}{\omega_*}\right)^{-2}$
p	$\frac{P}{\rho_i g}$	110.5
ζ	$\frac{1}{12g^2}h^2\omega^4$	$8.66\times10^{-4}\left(\frac{h}{h_*}\right)^2\left(\frac{\omega}{\omega_*}\right)^4$
σ	$\frac{2}{\pi^2 g^2(1-\nu)}h^2\omega^4$	$3\times10^{-3}\left(\frac{h}{h_*}\right)^2\left(\frac{\omega}{\omega_*}\right)^4$
ϖ	$\Pi\omega^{-1}$	...

TABLE 3. The non-dimensional parameters that appear in the scattering problem, together with their dependence on the physical variables ω, h and d. The characteristic values d_*, h_*, ω_* are given in table 2.

where $\mu^2 = \gamma^2 + \kappa^2$ and μ is the positive real root of the open-ocean dispersion relation (see § 5),

$$\mu \tanh \mu H = 1. \tag{2.17}$$

The parameter κ is $\kappa = \mu \sin\theta$, where θ is the angle of incidence to the ice sheet (see figure 1); $\theta = 0$ corresponds to normal incidence.

We next write

$$\hat{\phi}(x, y, z) = \phi^{inc}(x, y, z) + \phi^{sc}(x, y, z), \tag{2.18}$$

which introduces explicitly the scattered field, $\phi^{sc}(x, y, z)$, for which we may take

$$\phi^{sc}(x, y, z) = \phi(x, z)e^{i\kappa y}. \tag{2.19}$$

The y dependence is extracted explicitly as the ice sheet extends to $\pm$ infinity, and there is no variation in the ice sheet, or ocean, properties for fixed y.

In terms of the scattered field amplitude the potential equation becomes

$$\left(\frac{\partial^2}{\partial x^2} + \frac{\partial^2}{\partial z^2} - \kappa^2\right)\phi(x, z) = 0, \tag{2.20}$$

subject to

$$z = 0, \quad x < 0: \quad \phi + \phi_z = 0 \tag{2.21}$$

and

$$z = 0, \quad x > 0: \quad \mathscr{L}(\partial_x)[\phi_z(x, 0)] + \mathscr{M}(\partial_x)[\phi(x, 0)] = \Xi e^{i\gamma x}. \tag{2.22}$$

By subtracting out the incident field we have, in effect, translated the boundary-value problem into one where the ice sheet is vibrating; the parameter Ξ describes this

effect:

$$\Xi = \epsilon\mu^4 - (\zeta + \sigma + \delta\sigma)\mu^2 - 1 - p\kappa^2 + \frac{\sigma\zeta}{\epsilon}. \tag{2.23}$$

Also

$$\phi_z(x, H) = 0 \tag{2.24}$$

(or $\phi \to 0$ as $z \to \infty$ for the case of infinite depth). The edge conditions

$$\left(\partial_x^2 - \nu\kappa^2\right)\phi_z(0^+, 0) + \gamma^2 + \nu\kappa^2 = 0 \tag{2.25}$$

and

$$\left[\frac{\partial^2}{\partial x^2} - (2-\nu)\kappa^2 + \frac{\sigma+\zeta}{\epsilon}\right]\partial_x\phi_z(0^+, 0) + \mathrm{i}\gamma\left[\gamma^2 + (2-\nu)\kappa^2 - \frac{\sigma+\zeta}{\epsilon}\right] = 0, \tag{2.26}$$

are also required. To streamline formulae to come later, we have defined the operators

$$\mathscr{L}(\partial_x) = \epsilon\left(\frac{\partial^2}{\partial x^2} - \kappa^2\right)^2 + (\zeta + \sigma)\left(\frac{\partial^2}{\partial x^2} - \kappa^2\right) - p\kappa^2 + \delta - 1 + \frac{\sigma\zeta}{\epsilon} - \mathrm{i}\varpi \tag{2.27}$$

and

$$\mathscr{M}(\partial_x) = \delta\left[1 - \frac{\sigma\zeta}{\epsilon} - \sigma\left(\frac{\partial^2}{\partial x^2} - \kappa^2\right)\right]. \tag{2.28}$$

Note that, in the standard thin-plate theory (in which $\sigma = \zeta = 0$), $\mathscr{L}(\partial_x) = \epsilon\left(\partial_x^2 - \kappa^2\right)^2 - p\kappa^2 + \delta - 1$ and $\mathscr{M}(\partial_x) = \delta$, together with some simplifications of the edge conditions and Ξ. This particular case is the one we shall use for purposes of illustration in the scattering problem. But, if required, one can carry the analysis through for different plate models using the general formalism introduced above; for these other models, we need only introduce different forms for $\mathscr{L}$, $\mathscr{M}$, the edge conditions and Ξ.

This completes the formulation of the non-dimensional problem. Before continuing on to solve these equations, however, it is first helpful to describe various special cases and estimate typical values of the parameters of the problem.

3. Special cases

In certain limits of the parameters, the equations reduce to some models used previously in the ocean-wave problem. In this section, we briefly describe these special cases.

3.1. *Limits of H*

The two limiting cases in H are infinite depth, $H \to \infty$, and shallow water, $H \to 0$; occasional reference is made to these special cases later.

The shallow-water limit, $H \ll 1$, was treated by Evans & Davies (1968) in some detail; see also Keller & Goldstein (1953). The term 'shallow water' is slightly misleading: this is the limit when the ratio of water depth to incident wavelength is small. The water depth itself is not necessarily small and, for fixed depth and high frequency, one passes out of this limit ($H \sim \omega^2$).

None the less, the limiting situation $H \ll 1$ is important not only because the solution of the scattering problem can be found in closed form, but also because the

boundary-value problem itself can be cast more transparently: in the limit $H \to 0$, we adopt the expansion

$$\phi(x,z) \sim \psi(x) - \frac{(z-H)^2}{2}[\psi_{xx}(x) - \kappa^2\psi(x)], \tag{3.1}$$

which explicitly factors out the dependence on depth. Moreover, the scattered wave amplitude, $\psi(x)$, satisfies ordinary differential equations that account for the boundary conditions:

$$\psi_{xx} - \gamma^2\psi = 0 \quad \text{for } x < 0, \qquad \mathscr{L}(\psi_{xx} - \kappa^2\psi) + \frac{1}{H}\mathscr{M}\phi = 0 \quad \text{for } x > 0 \tag{3.2}$$

with $\gamma^2 = \kappa^2 - 1/H$. These equations are connected via the edge conditions, which are therefore automatically incorporated. We solve these equations by standard techniques (see Appendix B, § B.2) and this provides a useful check upon our analysis of the full problem. The terms involving $1/H$ may initially appear dominant; however in the shallow water limit $\mu = 1/\sqrt{H}$ and thus κ^2 is also $O(1/H)$.

The shallow-water theory has the great advantage that it is easily generalized to incorporate more complex phenomena, without the technicalities of the Wiener–Hopf approach. Thus it provides a useful avenue for exploring extra physical or geometrical effects.

3.2. *Thin-plate equation:* $\Sigma = \zeta = p = \varphi = \varpi = 0$

If we set all parameters to zero bar ϵ, δ and H, then we recover the standard thin-plate equation. This special case is perhaps the most important, and so we will discuss it in some detail. In particular, there are more special cases that arise in certain limits of ϵ and δ.

3.2.1. *Mass loading limit:* $\epsilon \ll 1$

As $\epsilon \to 0$, the elasticity of the ice sheet becomes small and we enter the mass-loading limit. This is the case, for example, if the ice sheet is very fragmented and the effective flexural rigidity is small, or as the ice thickness tends to zero.

For $\epsilon = 0$, we recover the mass loading model considered by Weitz & Keller (1950) and Peters (1950). This model was also used by Wadhams & Holt (1991) for frazil ice (although Newyear & Martin 1997 express reservations concerning its suitability).

The limit $\epsilon \to 0$ is, however, a singular one because the highest derivative then disappears from the plate equation. As a result, the mass-loading approximation always fails to approximate the plate theory at sufficiently high wavenumber (frequency) if ϵ is finite.

3.2.2. *Perfect transmission:* $\delta \to \infty$

In the limit $\delta \to \infty$ one recovers the open-ocean boundary condition. We pass into this limit when the density of the plate material is much less than the fluid density (which is not the case for ice and water), or if the ice sheet is very thin, or when the incident wave is of low frequency (see table 3). For all these cases, the waves are unaffected by the floating plate and so there is perfect wave transmission.

3.2.3. *Floating dock limit:* $\epsilon \gg 1$ *or* $\delta \ll 1$

Two limits lead to the 'floating-dock' problem in which the plate is effectively rigid (Heins 1948). The first limit is approached when the bending stiffness becomes large. Then $\epsilon \gg 1$, and the plate cannot flex. We also enter this limit when $\delta \ll 1$, which

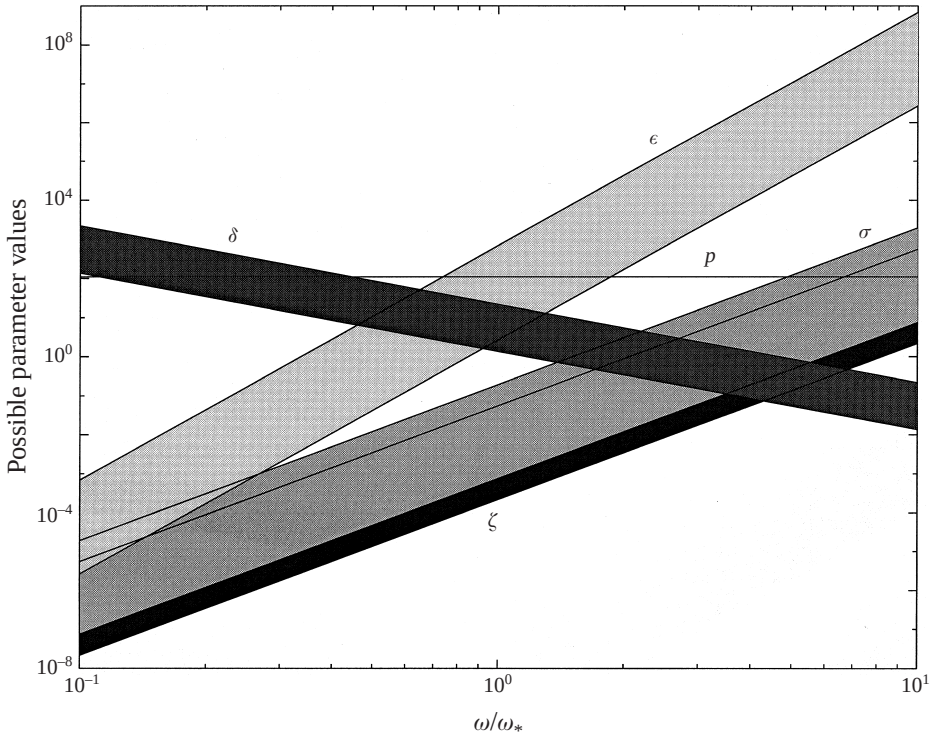

FIGURE 2. Parameter ranges plotted against (normalized) frequency. These ranges are given by the variation of h. Note that the ranges in σ and ζ overlap, and that p is constant.

arises if either the ice sheet is very thick, or if the plate were made of some other, very dense material. In both cases, the boundary condition is modified to $\phi_z = 0$.

The most important feature of this limit is that, because the plate is rigid, flexural waves cannot propagate. Hence reflection is always complete.

4. Dimensional considerations

Typical values of the physical constants and variables of the scattering problem are listed in tables 1 and 2. These all combine into the non-dimensional parameters listed in table 3. The ranges of these parameters are displayed in figure 2. From the typical values that we can extract from this table and figure, we may draw certain conclusions even without solving the equations.

First, for very small frequencies (long periods), $\delta \gg 1$ and $\epsilon \ll 1$; this corresponds to the limit of perfect transmission. At the other extreme, large frequency (short period), $\epsilon \gg 1$ and $\delta \ll 1$, implying that the elasticity of the ice sheet ultimately dominates and one obtains an effectively rigid ice sheet. The ocean waves are then perfectly reflected. Thus, as we traverse the wave spectrum, we pass from perfect transmission to total reflection. For values of h close to h_* the transition must occur for values of ϵ and δ of $O(1)$, which is therefore over a frequency range centred around $\omega = \omega_*$.

Second, over the whole range of values of ω, the Timoshenko–Mindlin parameters, σ and ζ, are typically very much smaller than ϵ. Thus, it would take an unusual selection of parameter values in order for these 'thick-plate' parameters to have any

effect upon the problem. This remains the case even if we use $h = 100\,\mathrm{m}$, a value suitable for an ice shelf or tongue. Note that, because ϵ, ζ and σ all have the same h dependence, it is only if one proceeds to very long periods that one could escape this feature of the problem (and not by changing the ice thickness). In other words, the Timoshenko–Mindlin model is unlikely to be very different from the thin-plate one, even for very thick ice sheets, as found earlier by Fox & Squire (1991). Hence the inclusion of ζ and σ in the scattering calculations is probably not necessary and for that reason we give no examples based on the Timoshenko–Mindlin model.

A physical effect that may prove to be important, on the other hand, is that resulting from the compressive stress. This stress is parameterized by p, which is independent of the physical variables. Moreover, for certain frequencies, this parameter can certainly be important (see figure 2). For this reason, we include p in the examples used in the scattering problem.

5. Wave propagation

We now move onto the scattering problem. The first step is to study wave propagation in the two regions separately. That is, in either the infinite open ocean, or a sea with an unending ice cover. This allows us to determine when waves will propagate in the two regions. Moreover, it leads us to uncover a simple criterion for complete reflection of waves with oblique incidence (Evans & Davies 1968). We do this for the non-dissipative problem (so $\varphi = \varpi = 0$) because in the scattering problem we will be more concerned with this case. However, at the end of this section, we also consider the attenuation of the wave amplitude due to our model dissipation.

5.1. *Open ocean*

For the open ocean, we take

$$\hat{\phi} = \frac{\cosh \mu(z-H)}{\cosh \mu H} \exp(\mathrm{i}\xi_{sea} x + \mathrm{i}\kappa y), \tag{5.1}$$

with $\mu^2 = \xi_{sea}^2 + \kappa^2$, or $\xi_{sea} = \mu\cos\theta$ and $\kappa = \mu\sin\theta$, where θ is the angle of incidence to the ice sheet (see figure 1). On applying the boundary condition (2.11), we find the dispersion relation, $\mu\tanh\mu H = 1$. This relation has a root on the real axis at $\mu = \mu_p$, for which $\xi_{sea} = \pm\sqrt{\mu_p^2 - \kappa^2} = \pm\gamma$. These are the propagating surface gravity waves; $\xi_{sea} = \gamma$ corresponds to a wave propagating to the right and we use the associated solution as the incident wave. In addition to these normal modes there is an infinite number of roots of the dispersion relation lying along the imaginary axis. The spectrum for normal incidence ($\theta = 0$) is illustrated in figure 3(*a*).

For later use, we define the dispersion function,

$$\mathscr{D}_{sea}(\xi_{sea}) = \mu(\xi_{sea})\tanh\mu(\xi_{sea})H - 1. \tag{5.2}$$

Note that we write the dispersion functions in terms of ξ rather than the total wavenumber Γ because of the forthcoming transform analysis.

5.2. *Ice-covered sea*

For ice-covered ocean, we take

$$\hat{\phi} = \frac{\cosh \Gamma(z-H)}{\cosh \Gamma H} \exp(\mathrm{i}\xi_{ice} x + \mathrm{i}\kappa y), \tag{5.3}$$

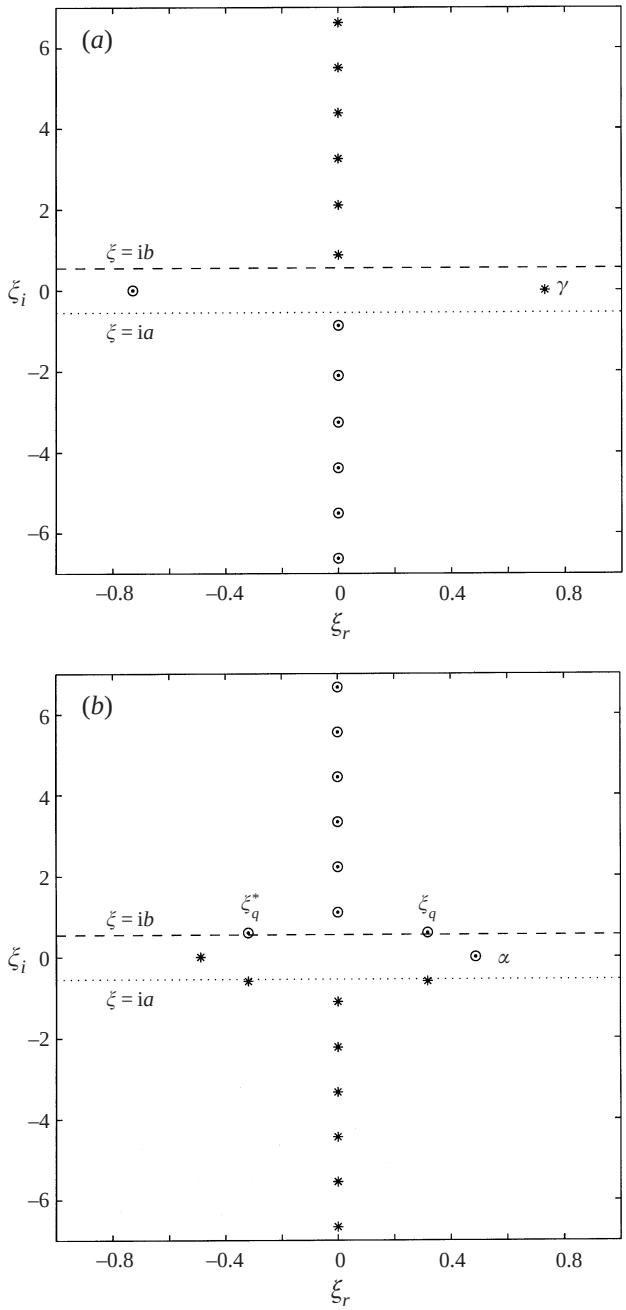

FIGURE 3. Normal-mode spectra for normal incidence ($\theta = 0$): (*a*) shows the open-sea spectrum and (*b*) the ice-covered ocean spectrum. The parameter values $H = 2$, $\epsilon = 10$, $\delta = 2$ and $\sigma = \zeta = p = \varpi = \varphi = 0$ are used. The encircled modes in the pictures are those onto which the scattered wave field can be projected (see Appendix A). The wavenumbers γ and α are those which arise for the right-going surface gravity waves. The horizontal dotted line, $\xi = -ia$, lies above the modes of either spectrum that are in the lower half-plane; the dashed line, $\xi = ia$, lies below any mode of either spectrum in the upper half-plane.

with $\Gamma^2(\xi_{ice}) = \xi_{ice}^2 + \kappa^2$, or equivalently $\xi_{ice} = \Gamma\cos\theta_T$ and $\kappa = \Gamma\sin\theta_T$, where θ_T is the angle of 'transmitted' waves. By using the plate equation we derive the dispersion relation

$$\mathscr{D}_{ice}(\xi_{ice}) = \mathscr{L}(\mathrm{i}\xi_{ice})\Gamma\tanh(\Gamma H) - \mathscr{M}(\mathrm{i}\xi_{ice}) = 0, \tag{5.4}$$

in which $\mathscr{L}$ and $\mathscr{M}$ are now simply functions rather than operators. More explicitly,

$$\mathscr{D}_{ice}(\xi_{ice}) =$$

$$\left[\epsilon\Gamma^4 - (\sigma+\zeta)\Gamma^2 - p\kappa^2 + \delta - 1 + \frac{\sigma\zeta}{\epsilon} - \mathrm{i}\varpi\right]\Gamma\tanh(\Gamma H) - \delta\left(1 - \frac{\sigma\zeta}{\epsilon} + \sigma\Gamma^2\right). \tag{5.5}$$

In the important special case of the thin plate with compression,

$$\mathscr{D}_{ice}^{TP}(\xi_{ice}) = \left(\epsilon\Gamma^4 - p\kappa^2 + \delta - 1\right)\Gamma\tanh(\Gamma H) - \delta = 0. \tag{5.6}$$

The dispersion relation (5.4) also has (for most physically relevant plate equations and without dissipation) a real solution for $\Gamma : \Gamma = \Gamma_p$. This gives the flexural waves with $\xi_{ice} = \pm\alpha = \pm\sqrt{\Gamma_p^2 - \kappa^2}$. In addition there is an infinite number of solutions for ξ_{ice} distributed along the imaginary axis, and a quartet of complex solutions; the spectrum for normal incidence is illustrated in figure 3(*b*). For future use, the member of the quartet lying in the first quadrant is denoted by ξ_q. Note that, in the limit of infinite depth, the discrete solutions along the imaginary axis are replaced by the branch cuts, $[\mathrm{i}\kappa,\ \mathrm{i}\infty)$ and $[-\mathrm{i}\kappa,\ -\mathrm{i}\infty)$.

When we restore dimensions we can plot frequency against wavenumber for the wave-like solution, $\Gamma = \Gamma_p(\omega/\omega_*)$. This is displayed in figure 4. The various curves in the two panels show the effect of varying h and d. In this figure, ζ and σ are non-zero. However, the curves appear unchanged if we explicitly set these parameters to zero, which emphasizes that the Timoshenko–Mindlin terms have little effect.

To bring out the effect of σ and ζ we plot phase speed, ω/k, in figure 5, where $k = \omega^2\Gamma_p/g$; these quantities are not non-dimensionalized in these figures or the ensuing discussion. For large frequency, the phase speed increases indefinitely (and unphysically) if $\sigma = \zeta = 0$. But when these parameters are included, the phase speed eventually levels off at a constant value (in fact, for ω well outside the physical range). This is the Rayleigh wave speed in the ice sheet, and its inclusion is one of the major successes of the Timoshenko–Mindlin model in structural acoustics. However, as pointed out in the last section, this extra feature is unlikely to have any effect in the ocean-wave scattering problem, and so Rayleigh waves apparently play no role in the fracture process.

5.3. *Critical reflection*

We now consider the right-going surface gravity wave with $\xi_{sea} = \gamma = \sqrt{\mu_p^2 - \kappa^2}$, and the right-going flexural wave for which $\xi_{ice} = \alpha = \sqrt{\Gamma_p^2 - \kappa^2}$. In either case, provided $\mu_p^2 > \kappa^2$ or $\Gamma_p^2 > \kappa^2$, there is a propagating wave. In the scattering problem, we are concerned with incoming ocean waves, and so we take $\mu_p^2 > \kappa^2$ as part of the characterization of the incident wave. This wave may be transmitted into the ice sheet, but as $x \to +\infty$, there will only be a propagating flexural wave if $\Gamma_p^2 > \kappa^2$, which is not automatic. Indeed, we may derive a version of Snell's law:

$$\kappa = \mu_p\sin\theta = \Gamma_p\sin\theta_T. \tag{5.7}$$

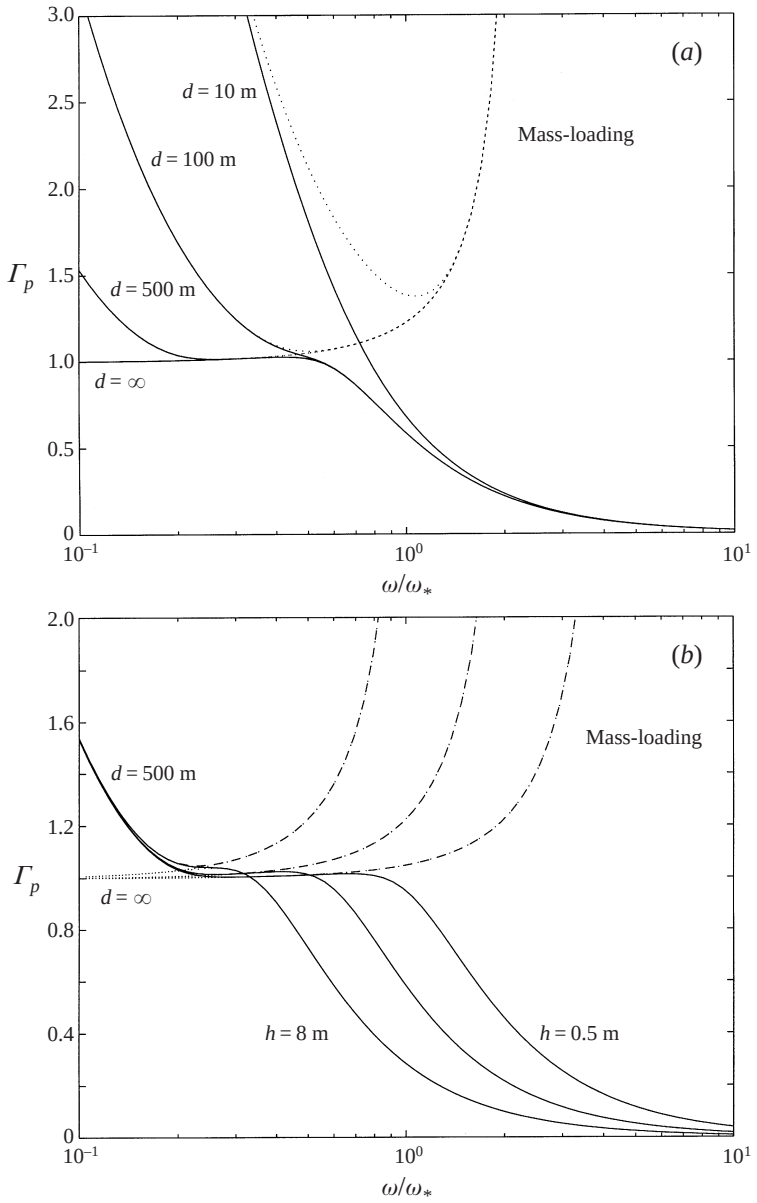

FIGURE 4. Propagating wavenumbers in ice-covered sea. (*a*) $\Gamma_p(\omega/\omega_*)$ for various values of d and $h = 2\,\mathrm{m}$; the dotted lines indicate the wavenumbers predicted by the mass-loading model. (*b*) $\Gamma_p(\omega/\omega_*)$ for various values of h (namely 0.5, 2 and 8 m) and $d = 500\,\mathrm{m}$; the dashed curves indicate the corresponding mass-loading model, and the dotted curves show the same results for infinite depth. ($p = \varpi = \varphi = 0$.)

Thus, the transmitted waves only propagate if

$$\Gamma_p > \mu_p \sin\theta \quad \text{or} \quad \theta < \theta_c, \tag{5.8}$$

where $\theta_c = \sin^{-1}(\Gamma_p/\mu_p)$. On the other hand, if $\theta > \theta_c$, then waves must be totally reflected at the ice edge.

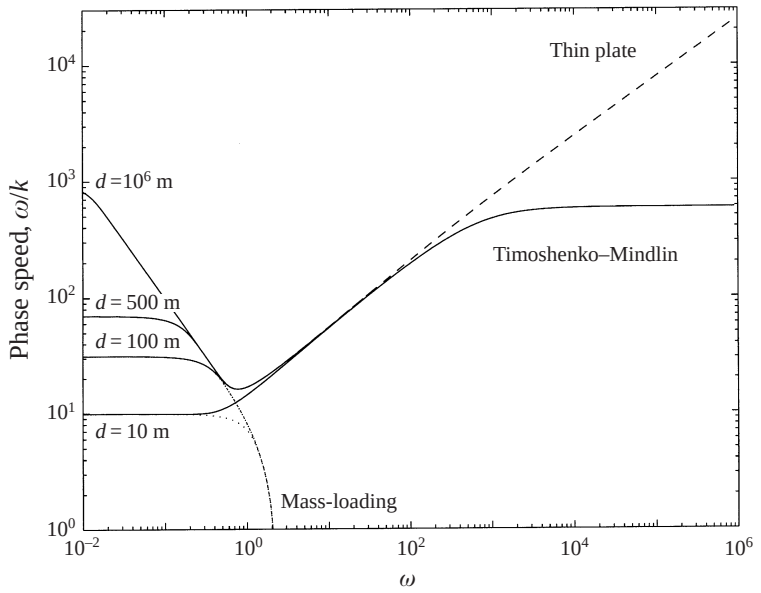

FIGURE 5. Phase speed, ω/k, where $k = \omega^2\Gamma_p/g$. The solid curves show the Timoshenko–Mindlin case, and the dashed lines indicate the thin-plate theory. Mass-loading predictions are included as dotted lines. In all three cases, four depths are included: $d = 10$, 100, 500 and 10^6 m. At low frequency, where the depth dependence is important, all three theories give identical predictions. The frequency range is extended well to the right in order to reveal the characteristic cut-off in the Timoshenko–Mindlin model at the Rayleigh wave speed.

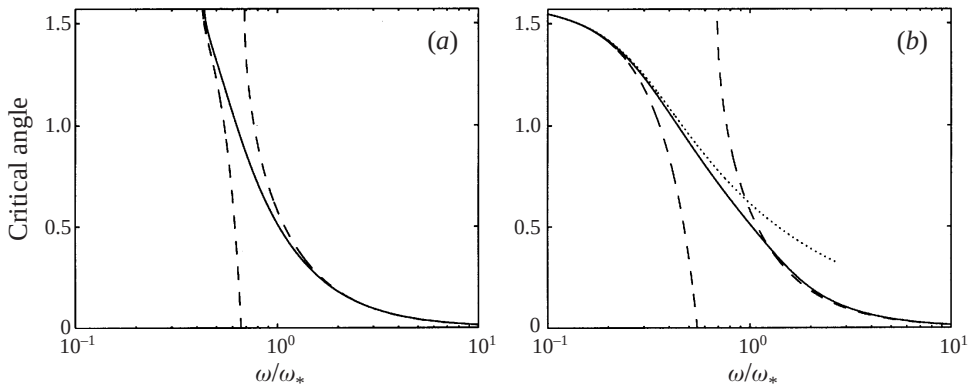

FIGURE 6. The critical angle versus frequency for $h = 1.5$ m. (*a*) The results for infinite depth with the exact solution as the solid line. The dashed lines are approximations to the critical angle θ_c: $\theta_c \sim \sin^{-1}\left(\delta/(\delta-1) - \epsilon\delta^6/(\delta-1)^5\right)$ for $\epsilon \ll \delta$, and $\theta_c \sim \sin^{-1}(\delta/\epsilon)^{1/5}$ for $\delta \ll \epsilon$. (*b*) The equivalent results for shallow water $d = 10$ m. Here, $\theta_c \sim \sin^{-1}\{\delta/(\delta-1)\,[1 - \epsilon\delta^2/(2H^2(\delta-1)^3)]\}$ for $\epsilon \ll \delta$. The dotted line is an approximation to θ_c that comes from a shallow-water approximation discussed in Appendix B, § B.2.

We illustrate the critical angles for the thin-plate equation in figure 6. In the shallow-water limit, we may derive an approximate formula for the cut-off (Evans & Davies 1968); this approximation is included in figure 6. The qualitative features of the cut-off were discussed by Evans & Davies (1968) and Fox & Squire (1994).

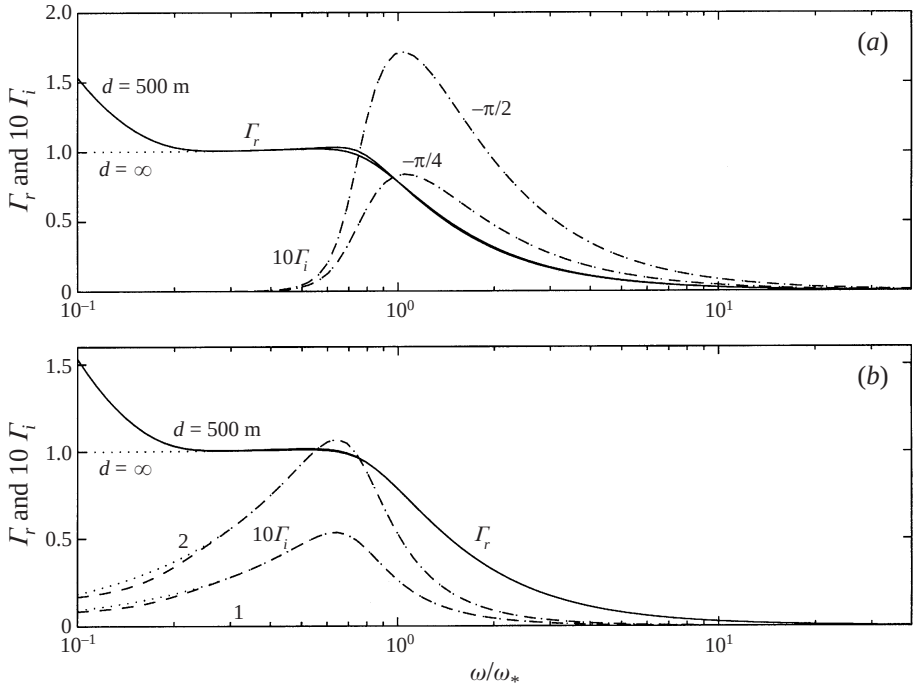

FIGURE 7. Wavenumber and damping rates for dissipative models: the solid curves show the wavenumber Γ_r as a function of frequency ω/ω_*; the dashed curves show the damping rate which is multiplied by 10 for the purposes of presentation. The plate thickness and ocean depth are $h = 1\,\mathrm{m}$ and $d = 500\,\mathrm{m}$. The dotted lines are the corresponding curves for infinite depth, which are only discernably different at very low frequency. (*a*) $\varphi = -\pi/4$ and $-\pi/2$ with $\varpi = 0$; (*b*) $\varphi = 0$ and $\Pi = 1\ \mathrm{s}^{-1}$ and $2\ \mathrm{s}^{-1}$.

5.4. *Attenuation lengths*

Finally we reintroduce dissipation in our model. In this instance, provided the dissipative terms are not too large, the spectra of the ice-covered ocean remains of a form like that in figure 3(*a*). However, the eigenvalues are moved by the addition of dissipation, and in particular, the eigenvalues $\Gamma = \pm\Gamma_p$ are shifted off the real axis. The right-propagating wave with $\Gamma = \Gamma_p$ is displaced into the upper half-plane, and $\Gamma = -\Gamma_p$ into the lower half-plane. Thus these waves attenuate as they propagate. None the less, for sufficiently small ϖ and φ, they remain the least-damped modes.

The attenuation length of a wave with frequency ω is given by $\mathrm{Im}(\Gamma^{-1})$ in our dimensionless notation, where Γ is the normal-mode wavenumber corresponding to Γ_p in the non-dissipative problem. The results are shown in figure 7.

Figure 7(*a*) shows the real and imaginary parts of the dimensionless wavenumber for $\varphi = -\pi/4$ and $-\pi/2$ (for dissipation one requires $\varphi < 0$) and with $\varpi = 0$, and (*b*) shows the same picture for $\varphi = 0$ and $\Pi = 1\,\mathrm{s}^{-1}$ and $2\,\mathrm{s}^{-1}$. Both (*a*) and (*b*) bear some similarities to figure 5 of Keller (1998) who used a rather more complicated model of dissipation but no elasticity in the ice. Note that the case $\varphi = -\pi/2$ corresponds to a purely imaginary flexural rigidity. That is, it models a dissipative effect rather than an elastic one. In other words, it might be possible to use this case as a dissipative model of frazil ice. In that context, the decrease of the real part of the wavenumber with frequency is consistent with observations of Newyear & Martin (1997). However, there was no observation of an ultimate decrease in $\mathrm{Im}(\Gamma)$ in those experiments as in

figure 7(*a*) (Keller's more complicated model also shows a decay in $\mathrm{Im}(\Gamma)$ at larger ω).

As we mentioned in the introduction, simple friction was used by Fox & Squire (1992) to improve the comparison of theory and observation of flexural waves. Because the two cases shown in figure 7 are quite similar, this is probably true also of the other model of dissipation.

6. Transform solution

The scattering problem falls into a class of mixed boundary-value problems that can be solved via the Wiener–Hopf technique (Noble 1958). This solution can be found for the general, modified Timoshenko–Mindlin plate equation. However, in view of the fact that most of the additional physics present in this formulation of the problem is not necessary (§ 5.2), we will only sketch out the solution from a formal standpoint. Practically, we take the thin-plate equation with a lateral compressive stress as an illustrative model.

6.1. *The functional equation*

We simplify the boundary-value problem formulated above by applying Fourier transforms in the x-coordinate. First, we define the one-sided transforms of $\phi(x,z)$:

$$\Phi_+(\xi,z)=\int_0^\infty \phi(x,z)\mathrm{e}^{\mathrm{i}\xi x}\mathrm{d}x \quad \text{and} \quad \Phi_-(\xi,z)=\int_{-\infty}^0 \phi(x,z)\mathrm{e}^{\mathrm{i}\xi x}\mathrm{d}x. \tag{6.1}$$

Since the scattered wave field may have finite amplitude at $x=\pm\infty$ we need to interpret these transforms with a little care. In particular, the integrals in (6.1) only converge for certain values of ξ, and the transforms are not then defined in the same parts of the complex ξ-plane (Φ_+ converges for $\mathrm{Im}(\xi)>0$ and Φ_- for $\mathrm{Im}(\xi)<0$). This leads to a technical difficulty that is surmounted in Appendix A. The outcome of that discussion is that, despite apparent divergences, we may define the functions $\Phi_\pm(\xi,z)$ over the whole of the complex ξ-plane. Moreover, $\Phi_-(\xi,z)$ is analytic (in ξ) over the region S_-, and $\Phi_+(\xi,z)$ is analytic in S_+, where $S_\pm$ are illustrated in figure 8. More specifically, the '$-$ region', S_-, is the strip $\mathrm{Im}(\xi)<a$, with two pieces cut out so as to remove the points $\xi=\gamma$ and $\xi=\alpha$. Similarly, the '$+$ region', S_+, is the strip $-a<\mathrm{Im}(\xi)$, except for portions that remove $\xi=-\gamma$ and $\xi=-\alpha$. The meaning of the positive constant a is illustrated in figure 3; it is a constant that bounds the eigenvalues of both open ocean and ice-covered sea with finite imaginary part away from the real axis. This analytic structure (analyticity over $S_\pm$) provides the essential meaning of the $\pm$ subscripts.

Given these details, we can then define the function,

$$\Phi(\xi,z)=\Phi_+(\xi,z)+\Phi_-(\xi,z), \tag{6.2}$$

which is more like the usual Fourier transform. For the dissipative problem, there is no difficulty in defining $\Phi_+(\xi,z)$ because the transmitted wave dissipates to zero amplitude as it propagates to $x\to\pm\infty$. However, the complication associated with the reflected wave remains, and we must still define regions of analyticity like $S_\pm$.

We first apply the half-range Fourier transforms to equation (2.20):

$$\Phi_{\pm zz}-(\xi^2+\kappa^2)\Phi_\pm=\pm[\phi_x(0,z)-\mathrm{i}\xi\phi(0,z)] \tag{6.3}$$

or

$$\Phi_{zz}-(\xi^2+\kappa^2)\Phi=0. \tag{6.4}$$

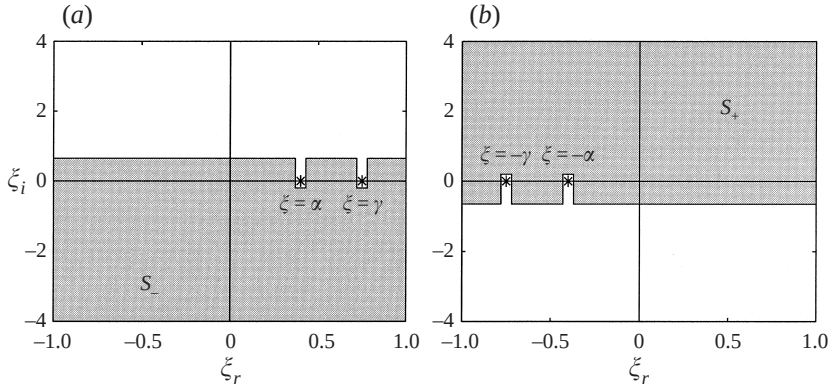

FIGURE 8. The strips $S_\pm$ over which the $\pm$ functions must be analytic, respectively, when there is no dissipation. The two strips overlap in a region running parallel to the real axis.

Solutions of (6.4) are found in terms of hyperbolic functions, after applying the boundary condition at $z = H$, we find

$$\Phi(\xi, z) = I(\xi)\frac{\cosh \Gamma(z - H)}{\cosh \Gamma H}, \tag{6.5}$$

where $\Gamma(\xi) = \sqrt{\xi^2 + \kappa^2}$ and the function $I(\xi)$ is as yet unknown. (To interpret the multi-valued function $\Gamma(\xi)$, we take $\Gamma(\xi)$ to have the branch cuts, $[\mathrm{i}\kappa,\ \mathrm{i}\infty)$ and $[-\mathrm{i}\kappa,\ -\mathrm{i}\infty)$.)

Next, we consider the boundary conditions on $z = 0$. From the condition along $x < 0$, we may derive

$$\Phi_{-z}(\xi, 0) + \Phi_-(\xi, 0) = 0. \tag{6.6}$$

Hence,

$$\Phi_{+z}(\xi, 0) + \Phi_+(\xi, 0) = \Phi_z(\xi, 0) + \Phi(\xi, 0) \equiv -\mathscr{D}_{sea}(\xi)I(\xi). \tag{6.7}$$

That is,

$$I(\xi) = -\frac{\Phi_{+z}(\xi, 0) + \Phi_+(\xi, 0)}{\mathscr{D}_{sea}(\xi)}, \tag{6.8}$$

where the open-ocean dispersion function $\mathscr{D}_{sea}(\xi) = \mu(\xi)\tanh \mu(\xi)H - 1$, as in equation (5.2).

To incorporate the plate equation, we consider the quantity,

$$\Delta = \mathscr{L}(\partial_x)[\phi_z(x, 0)] + \mathscr{M}(\partial_x)[\phi(x, 0)]. \tag{6.9}$$

Using (2.22) one deduces that $\Delta = \Xi \mathrm{e}^{\mathrm{i}\gamma x}$ in $x > 0$. If we take the half-range '+, −' transforms, then

$$\hat{\Delta}_\pm(\xi) = \mathscr{L}(\mathrm{i}\xi)\Phi_{\pm z}(\xi, 0) + \mathscr{M}(\mathrm{i}\xi)\Phi_\pm(\xi, 0) \mp \epsilon P^\pm(\xi), \tag{6.10}$$

where the hat on Δ denotes the Fourier transform, and $\mathscr{L}(\mathrm{i}\xi)$ and $\mathscr{M}(\mathrm{i}\xi)$ are the transformed operators (now merely algebraic factors). The final term on the right-hand side of (6.10) corresponds to the contribution from the half-range transforms at the origin (and appears by virtue of various integrations by parts). Crucially this involves the plate displacement and its derivatives evaluated at the edge. For the

thin-plate equation with a lateral compressive stress:

$$P^{\pm}(\xi) = \phi_{zxxx}(0^{\pm},0) - \mathrm{i}\xi\phi_{zxx}(0^{\pm},0) - (2\kappa^2+\xi^2)\phi_{xz}(0^{\pm},0) + \mathrm{i}\xi(2\kappa^2+\xi^2)\phi_z(0^{\pm},0). \tag{6.11}$$

When we add the two half-range transforms, we find

$$\hat{\Delta}_+(\xi) + \hat{\Delta}_-(\xi) = \mathscr{L}(\mathrm{i}\xi)\Phi_z(\xi,0) + \mathscr{M}(\mathrm{i}\xi)\Phi(\xi,0) - \epsilon[P^+(\xi) - P^-(\xi)]. \tag{6.12}$$

On exploiting the boundary condition on $x > 0$ we also find that

$$\hat{\Delta}_+(\xi) + \hat{\Delta}_-(\xi) = -\frac{\Xi}{\mathrm{i}(\gamma+\xi)_+} + [\mathscr{L}(\mathrm{i}\xi) - \mathscr{M}(\mathrm{i}\xi)]\Phi_{-z}(\xi,0) + \epsilon P^-(\xi), \tag{6.13}$$

where the subscript on $(\gamma+\xi)_+$ is added to remind us that this term is derived assuming that $\mathrm{Im}(\xi) > 0$, but has been analytically continued over the whole complex plane (which makes it a '+' function).

We now put these two results together to obtain the *functional equation*,

$$\epsilon P^+(\xi) + [\mathscr{L}(\mathrm{i}\xi) - \mathscr{M}(\mathrm{i}\xi)]\Phi_{-z}(\xi,0) - \frac{\Xi}{\mathrm{i}(\xi+\gamma)_+} = \frac{\mathscr{D}_{ice}(\xi)}{\mathscr{D}_{sea}(\xi)}[\Phi_{+z}(\xi,0) + \Phi_+(\xi,0)], \tag{6.14}$$

where $\mathscr{D}_{ice}(\xi)$ is the ice-covered ocean dispersion function, as defined in (5.4). From here on we only encounter $P^+(\xi)$ and henceforth we write this as $P(\xi)$.

In addition, we have the relation,

$$\mathscr{M}(\mathrm{i}\xi)\Phi_+(\xi,0) = \epsilon P(\xi) - \mathscr{L}(\mathrm{i}\xi)\Phi_{+z}(\xi,0) - \frac{\Xi}{\mathrm{i}(\gamma+\xi)_+}, \tag{6.15}$$

which (in principle) allows us to write the '+' function on the right of (6.14) solely in terms of $\Phi_{+z}(\xi,0)$. In other words, that equation relates $\Phi_{-z}(\xi,0)$ and $\Phi_{+z}(\xi,0)$; because $\phi_z(x,0)$ is directly related to the vertical displacement of the fluid surface, these functions are the transforms of the free-surface and plate displacements.

Equation (6.14) contains all the information regarding the boundary conditions and relates those functions that are currently unknown, namely $\Phi_{\pm z}(\xi,0)$. This is our functional equation. Once we solve this functional equation we can determine $I(\xi)$ and then the solution everywhere through a suitable inverse transform (see Appendix A).

6.2. *Splitting*

We now follow conventional, Wiener–Hopf methodology (e.g. Noble 1958). This involves separating the functional equation into a right-hand side that is a + function, and a left-hand piece which is a − function. Because these functions also have a common, overlapping region of analyticity (a cut strip parallel to the real axis; see figure 8), they are equal to a unique analytic function, $E(\xi)$, within that strip. By analytic continuation this function must also be analytic over the lower half-plane, where it equals the − function, and in the upper half-plane, where it is identical to the + function. In other words, $E(\xi)$ is an entire function. But, by the same argument, the $\pm$ functions equal $E(\xi)$ over the whole complex plane and so these functions must also be analytic everywhere. This remains true even as $|\xi| \to \infty$, and so (by Liouville's Theorem) $E(\xi)$ must be a polynomial in ξ. Up to some further technicalities, this allows us to find the unknown transforms analytically, and amounts to the resolution of the scattering problem.

Let

$$\mathscr{K}(\xi) = -\frac{\mathscr{D}_{ice}(\xi)}{\mathscr{D}_{sea}(\xi)}. \tag{6.16}$$

The crucial step in the Wiener–Hopf technique is the factorization of the function $\mathscr{K}(\xi)$ into a product of $\pm$ functions, $\mathscr{K}_+(\xi)\mathscr{K}_-(\xi)$. The split functions $\mathscr{K}_\pm$ have the important property that they have the same analyticity properties as $\Phi_\pm(\xi, z)$, and, moreover, have no zeros in $S_\pm$ respectively. Further details of the explicit factorization are given in Appendix B. One useful detail is that we can choose the factorization such that $\mathscr{K}_+(\xi) = \mathscr{K}_-(-\xi)$.

The functional equation (6.14) is rewritten as

$$\frac{1}{\mathscr{K}_-(\xi)}\{\epsilon P(\xi) + [\mathscr{L}(\mathrm{i}\xi) - \mathscr{M}(\mathrm{i}\xi)]\Phi_{-z}(\xi, 0)\} + \frac{\Xi}{\mathrm{i}(\xi+\gamma)_+}\left[\frac{1}{\mathscr{K}_+(\gamma)} - \frac{1}{\mathscr{K}_-(\xi)}\right]$$
$$= -\mathscr{K}_+(\xi)[\Phi_{+z}(\xi, 0) + \Phi_+(\xi, 0)] + \frac{\Xi}{\mathrm{i}(\xi+\gamma)_+\mathscr{K}_+(\gamma)}. \tag{6.17}$$

Note that we have added a term to both sides of (6.17) that has the effect of cancelling the pole in $(\gamma+\xi)_+^{-1}$ at $\xi = -\gamma$; this ensures the analyticity of left-hand side of (6.17) in S_-. That left-hand side is, therefore, a '$-$' function and the right-hand side is a '$+$' function, as desired. Both sides share the common region of analyticity (the intersection of S_+ and S_-) and are thus equal to the polynomial, $E(\xi)$.

To determine that entire function, we consider the limit $|\xi| \to \infty$. Because the highest x-derivative in the plate equation is ∂_x^4, $\mathscr{K}(\xi) \sim \xi^4$ in this limit, and so $\mathscr{K}_\pm(\xi) \sim \xi^2$. Moreover, $\Phi_{\pm z} \sim \xi^{-1}$, which follows from integrating by parts. Hence we deduce that both sides of the functional equation are $O(\xi)$ as $|\xi| \to \infty$. Thus $E(\xi) = A\xi + B$, where A and B are constants to be determined.

This line of argument leads to the two relations

$$[\mathscr{L}(\mathrm{i}\xi) - \mathscr{M}(\mathrm{i}\xi)]\Phi_{-z}(\xi, 0) = (A\xi + B)\mathscr{K}_-(\xi) - \epsilon P(\xi) - \frac{\Xi}{\mathrm{i}(\xi+\gamma)_+}\left[\frac{\mathscr{K}_-(\xi)}{\mathscr{K}_+(\gamma)} - 1\right] \tag{6.18}$$

and

$$\Phi_{+z}(\xi, 0) + \Phi_+(\xi, 0) = -\frac{A\xi + B}{\mathscr{K}_+(\xi)} + \frac{\Xi}{\mathrm{i}(\xi+\gamma)_+\mathscr{K}_+(\gamma)\mathscr{K}_+(\xi)}. \tag{6.19}$$

On using (6.15) the second of these is further written as

$$[\mathscr{L}(\mathrm{i}\xi) - \mathscr{M}(\mathrm{i}\xi)]\Phi_{+z}(\xi, 0) = \epsilon P(\xi) + \frac{\mathscr{M}(\mathrm{i}\xi)(A\xi + B)}{\mathscr{K}_+(\xi)} - \frac{\Xi}{\mathrm{i}(\gamma+\xi)_+}\left[\frac{\mathscr{M}(\mathrm{i}\xi)}{\mathscr{K}_+(\gamma)\mathscr{K}_+(\xi)} + 1\right]. \tag{6.20}$$

6.3. *Incorporating the edge conditions*

The functional equation (6.14), and its solutions (6.18) and (6.20), contain the quantity $P(\xi)$, which consists of the plate displacement $\phi_z(x, 0)$, and three derivatives of it, evaluated at the plate edge. These quantities are not currently known, and we employ the edge conditions (2.25) and (2.26) to eliminate the second and third derivative of $\phi_z(x, 0)$. Formally, this reduces $P(\xi)$ to

$$P(\xi) = P_0(\xi) + P_1(\xi)\phi_z(0^+, 0) + P_2(\xi)\phi_{zx}(0^+, 0). \tag{6.21}$$

In particular, for the thin-plate model with lateral compression,

$$P(\xi) = \mathrm{i}\xi[(1-\nu)\kappa^2 - \mu^2] - [\mu^2 + \kappa^2(1-\nu)]\mathrm{i}\gamma + \mathrm{i}\xi[\xi^2 + (2-\nu)\kappa^2]\phi_z(0^+,0) - (\xi^2 + \nu\kappa^2)\phi_{xz}(0^+,0). \quad (6.22)$$

The remaining two variables, $\phi_z(0^+,0)$ and $\phi_{xz}(0^+,0)$, are not determined by the edge conditions and constitute two unknown quantities in $P(\xi)$. Hence, together with the constants A and B, there are four unknowns in the solutions (6.18) and (6.20). But, that solution provides the combinations $[\mathscr{L}(\mathrm{i}\xi) - \mathscr{M}(\mathrm{i}\xi)]\Phi_{\pm z}(\xi)$. Hence to determine the transforms of the displacement, we further must divide by the quantity, $\mathscr{L}(\mathrm{i}\xi) - \mathscr{M}(\mathrm{i}\xi)$, which introduces poles into $\Phi_{\pm z}(\xi)$ at the zeros of $\mathscr{L}(\mathrm{i}\xi) - \mathscr{M}(\mathrm{i}\xi)$. That function is a fourth-order polynomial with the four zeros, $\xi = \chi_j$, $j = 1,\ldots,4$. For our illustrative model,

$$\chi_{1,2} = \pm\left[\left(\frac{1+p\kappa^2}{\epsilon}\right)^{1/2} - \kappa^2\right]^{1/2}, \text{ and } \chi_{3,4} = \pm\mathrm{i}\left[\left(\frac{1+p\kappa^2}{\epsilon}\right)^{1/2} + \kappa^2\right]^{1/2}. \quad (6.23)$$

The zeros χ_2 and χ_4 lie in the '–' region, and χ_1 and χ_3 are in S_+. Thus, $\Phi_{-z}(\xi,0)$ is not actually analytic in S_- unless

$$(A\xi + B)\mathscr{K}_-(\xi) - \epsilon P(\xi) - \frac{\Xi}{\mathrm{i}(\xi+\gamma)_+}\left[\frac{\mathscr{K}_-(\xi)}{\mathscr{K}_+(\gamma)} - 1\right] = 0 \quad (6.24)$$

when $\xi = \chi_2$ and χ_4. Similarly, $\Phi_{+z}(\xi,0)$ is not analytic in S_+ unless

$$\epsilon P(\xi) + \frac{\mathscr{M}(\mathrm{i}\xi)(A\xi+B)}{\mathscr{K}_+(\xi)} - \frac{\Xi}{\mathrm{i}(\gamma+\xi)_+}\left[\frac{\mathscr{M}(\mathrm{i}\xi)}{\mathscr{K}_+(\gamma)\mathscr{K}_+(\xi)} + 1\right] = 0 \quad (6.25)$$

for $\xi = \chi_1$ and χ_3. In fact, since $\mathscr{K}_+(\chi_j)\mathscr{K}_-(\chi_j) = -\mathscr{M}(\mathrm{i}\chi_j)$, both constraints can be written in the concise form

$$(A\xi+B)\mathscr{K}_-(\xi) - \epsilon\left[P_1(\xi)\phi_z(0^+,0) + P_2(\xi)\phi_{zx}(0^+,0)\right] = \frac{\Xi}{\mathrm{i}(\xi+\gamma)_+}\left[\frac{\mathscr{K}_-(\xi)}{\mathscr{K}_+(\gamma)} - 1\right] + \epsilon P_0(\xi) \quad (6.26)$$

at $\xi = \chi_j$, $j = 1,\ldots,4$. In order to satisfy these constraints, we must fix the values of the four unknowns, $\phi_z(0^+,0)$, $\phi_{zx}(0^+,0)$, A and B (that is, we solve four simultaneous algebraic equations).

With the edge behaviour and the polynomial, $A\xi + B$, fully specified, we have the solution to the Wiener–Hopf problem and we are in a position to compute $\phi(x,z)$ through the inverse transform.

7. Reflection and transmission coefficients

The far-field behaviour of the scattered potential is given by asymptotic considerations of the inverse transform

$$\phi(x,z) = \frac{1}{2\pi}\int_C \Phi(\xi,z)\mathrm{e}^{-\mathrm{i}\xi x}\mathrm{d}\xi \quad \text{as } x \to \pm\infty. \quad (7.1)$$

The path C in the inverse transform runs from $-\infty$ to $+\infty$ and is indented above $\xi = -\gamma$ and $-\alpha$, then below $\xi = \gamma$ and α (see Appendix A). We evaluate this integral after closing the contour C by adding arcs enclosing the entire either lower or upper half-plane. In these half-planes the functions to be inverted have an infinite number

of poles, and so the inverse transforms are expressible as infinite sums (see Evans & Davies 1968).

In the non-dissipative problem, as $x \to -\infty$, one particular residue dominates the sum; this corresponds to the pole at $\xi = \gamma$ and furnishes the reflected wave. For $x \to \infty$, a second pole dominates at $\xi = -\alpha$, provided this wavenumber is real, and this generates the transmitted wave.

Such calculations lead to the far-field form of the scattered wave amplitude, which is given explicitly in terms of the reflection and transmission coefficients, R and T:

$$\phi(x,z) \sim R\exp(-\mathrm{i}\gamma x)\frac{\cosh\mu(z-H)}{\cosh\mu H} \quad \text{as} \quad x \to -\infty \tag{7.2}$$

and

$$\phi(x,z) \sim T\exp(+\mathrm{i}\alpha x)\frac{\cosh\Gamma_p(z-H)}{\cosh\Gamma_p H} \quad \text{as} \quad x \to +\infty. \tag{7.3}$$

If α is not real, then there is no transmitted wave that propagates through the plate. In that circumstance, $|R| = 1$. However, T is not necessarily zero. In fact, one can still construct the leading contribution to the far-field form of the scattered wave even if α is imaginary. This corresponds to an exponentially decaying disturbance with a form similar to (7.3). In other words, T no longer has the meaning of a transmission coefficient, but is the amplitude of the least-decaying spatial mode.

The coefficients R and T in (7.2), (7.3) are given explicitly by

$$R = \frac{\mathrm{i}}{\mathscr{K}_+(\gamma)\mathscr{D}'_{sea}(\gamma)}\left[A\gamma + B - \frac{\Xi}{2\mathrm{i}\gamma\mathscr{K}_+(\gamma)}\right] \tag{7.4}$$

and

$$T = -\frac{\mathrm{i}\mathscr{K}_+(\alpha)}{\mathscr{D}'_{ice}(\alpha)}\left[A\alpha - B + \frac{\Xi}{\mathrm{i}(\gamma-\alpha)\mathscr{K}_+(\gamma)}\right]. \tag{7.5}$$

In our illustrative example there are formulae for $|\mathscr{K}_+(\gamma)|^2$ and $|\mathscr{K}_+(\alpha)|^2$ (see Appendix A) that lead to

$$|R| = \left|\frac{(\alpha-\gamma)}{(\alpha+\gamma)\Xi}\ [2\mathrm{i}\gamma\mathscr{K}_+(\gamma)(A\gamma+B) - \Xi]\right| \tag{7.6}$$

and

$$|T| = \frac{2}{(\alpha+\gamma)}\sqrt{\frac{\alpha\gamma\mathscr{D}'_{sea}(\gamma)}{|\Xi|\mathscr{D}'_{ice}(\alpha)\mathscr{D}_{sea}(\alpha)}}\,|[\mathrm{i}(\gamma-\alpha)\mathscr{K}_+(\gamma)(A\alpha-B)+\Xi]|\,. \tag{7.7}$$

Hence, to evaluate these coefficients, we need only compute $\mathscr{K}_\pm(\xi)$ at $\xi = \gamma$, $\xi = \chi_1$ and $\xi = \chi_2$ ($\xi = \chi_3$ and $\xi = \chi_4$ are the complex conjugates), and then solve the algebraic system (6.26) for A and B.

For the dissipative problem, the calculation is slightly different. In this case, α is always complex even if it corresponds to a transmitted wave. Provided it is the least-damped mode, however, it remains the dominant contribution to the sum of residues and we again emerge with the form of the transmitted wave in (7.3).

7.1. *Power flow*

For non-dissipative ice sheets there is a further relation between the reflection and transmission coefficients that corresponds to a 'power flow theorem' (cf. Keller &

Weitz 1953; Evans & Davies 1968; Wadhams 1986). This relation derives from the identity

$$\int_{-\infty}^{\infty}\int_{0}^{H}\left[\hat{\phi}(\partial_x^2+\partial_z^2-\kappa^2)\hat{\phi}^*-\hat{\phi}^*(\partial_x^2+\partial_z^2-\kappa^2)\hat{\phi}\right]\,\mathrm{d}x\mathrm{d}z=0, \tag{7.8}$$

which follows from equation (2.20). By applying Green's Theorem to the integral, we find

$$\mathrm{Im}\left(\int_0^H \hat{\phi}^*(x,z)\hat{\phi}_x(x,z)\Big]_{x\to-\infty}^{x\to+\infty}\mathrm{d}z-\int_0^\infty \hat{\phi}^*(x,0)\hat{\phi}_z(x,0)\mathrm{d}x\right)=0, \tag{7.9}$$

on account of the boundary conditions along $z=H$ and $z=0$, $x<0$.

The first integral in (7.9) can be evaluated explicitly in terms of the transmission and reflection coefficients. This leaves the integral along the plate to deal with. By using the plate equation and edge conditions we eventually eliminate all terms but one which can be evaluated in the limit as $x\to\infty$. This term also involves the transmission coefficient. The net result of these manipulations is the formula

$$\mathrm{Re}\left[(|R|^2-1)\mathscr{D}'_{sea}(\gamma)+|T|^2\frac{\Gamma_p}{\delta}\mathscr{D}'_{ice}(\alpha)\tanh\Gamma_p H\right]=0 \tag{7.10}$$

in the special case of the thin-plate model.

The power-flow theorem (7.10) can be thought of as a generalization of the relation $|R|^2+|T|^2=1$ familiar in electromagnetic wave theory. In that theory there is no coefficient in front of $|T|^2$ because transmission amplitude and transmitted power correspond to within a simple numerical factor. This is not true for flexural waves, and the relation between transmitted amplitude and power is encapsulated in (7.10). Nevertheless, the fractional transmitted power is still $1-|R|^2$.

When α is real, equation (7.10) is also real and can be shown to be consistent with (7.6) and (7.7). If α is imaginary, then all the incident power is reflected and (7.10) reduces to $|R|=1$. The proportion of scattered power transmitted into the ice-covered region is then zero, but this does not signify that $|T|^2$ is zero. Rather, the term multiplying $|T|^2$ in (7.10) is now purely imaginary (and T corresponds to the amplitude of a spatially decaying disturbance).

The power-flow result is valid for all edge conditions that do not introduce energy to the system; similar relations hold for more general plate equations. If terms appeared in (7.10) that corresponded to edge terms, then the edge conditions would not conserve energy and those terms would represent input of power at the ice edge.

Note that a verification of the power-flow relation is not an absolute check of numerical computations: Many numerical algorithms satisfy power-flow theorems exactly, but can still fail to solve the problem accurately (e.g. Craster 1998; Kriegsmann 1999). Thus, this verification is not always a good measure of how accurately a particular physical problem is solved, but simply confirms the internal consistency of the solution procedure.

8. Numerical results

Numerical computations of the reflection and transmission coefficients are shown in figures 9–12. In all figures the ice sheet thickness is 1.5 m.

As shown in figures 9(*a*) and 10(*a*), and in line with our dimensional arguments of § 4, as $\omega\to 0$ we enter the limit of perfect transmission, and as $\omega\to\infty$ one enters the floating dock limit with total reflection. With oblique incidence (figures 9*b* and 10*b*),

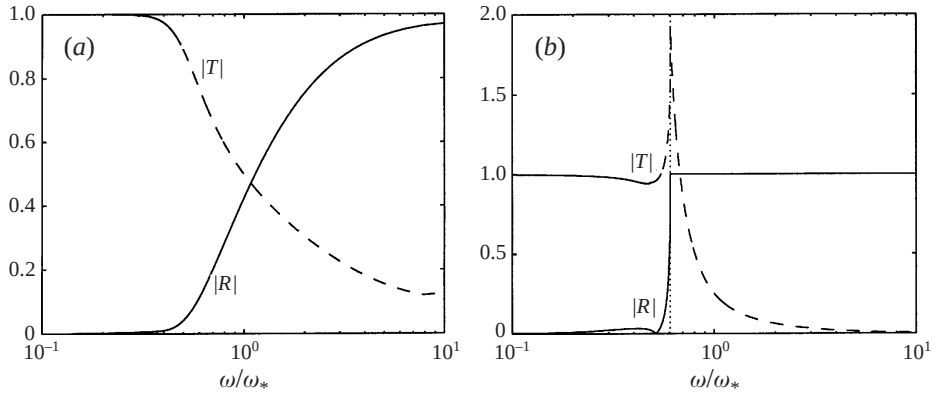

FIGURE 9. Absolute values of coefficients of reflection, $|R|$ (solid lines), and transmission, $|T|$ (dashed lines), for infinite depth: (*a*) $\theta = 0$ and (*b*) $\theta = \pi/3$. The vertical dotted line in (*b*) corresponds to the cut-off frequency.

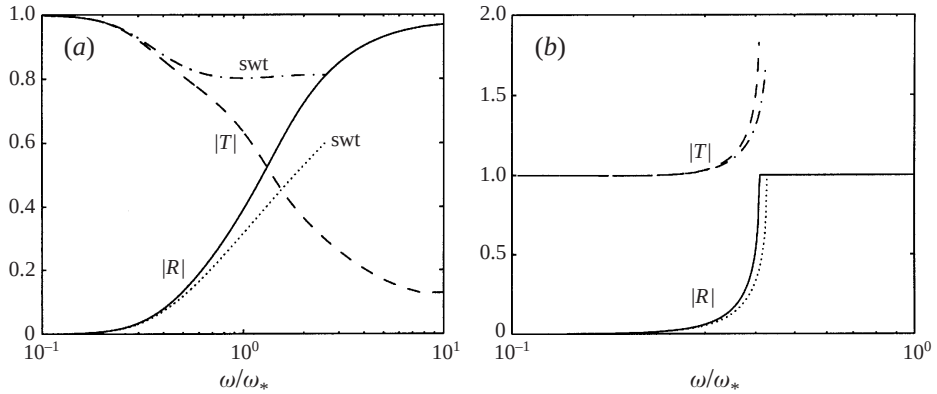

FIGURE 10. Absolute values of coefficients of reflection, $|R|$ (solid lines), and transmission, $|T|$ (dashed lines), for shallow water ($d = 10\,\mathrm{m}$): (*a*) $\theta = 0$ and (*b*) $\theta = \pi/3$. Approximate solutions using the shallow-water theory are also shown (labelled swt and drawn as dotted and dash-dotted lines); this limit breaks down at high frequencies. Note that the presence of a cut-off for obliquely incident waves restores the accuracy of the shallow-water approximation over that frequency range.

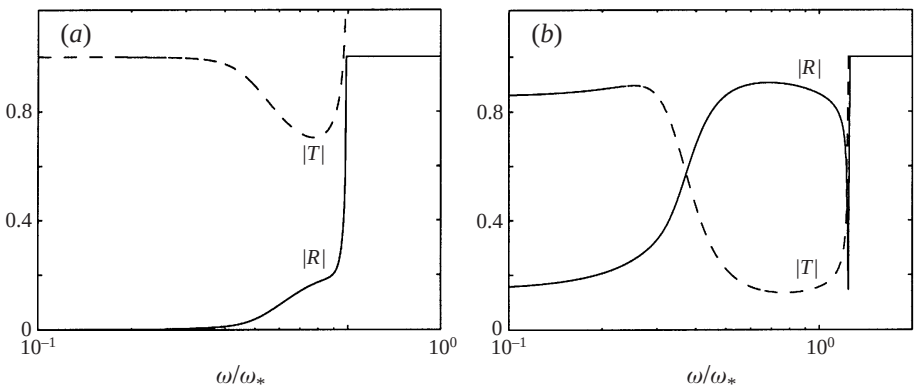

FIGURE 11. Absolute values of coefficients of reflection, $|R|$ (solid lines), and transmission, $|T|$ (dashed lines), for depth $d = 100\,\mathrm{m}$ for (*a*) $p = 0$ and (*b*) $p = 110.5$.

this view changes somewhat because there is now a cut-off frequency at the critical angle, above which there is no transmission.

Note that $|T|$ is larger than unity close to the cut-off wavelength. This is because $|T|$ is not the proportion of scattered power transmitted into the ice sheet, but the magnitude of the amplitude of the transmitted wave. The substantial peak in $|T|$ at near-critical angles suggests that the transmitted wave attains a significantly larger amplitude if generated in that direction (this is clearly seen for the shallow-water solution in Appendix B, § B.2; see (B 14)). In other words, transmitted waves that propagate almost parallel to the ice edge may be the most destructive to the ice sheet and primarily responsible for fracture. Note that the maximal values of $|T|$ are easily extracted from (7.7) because, at the cut-off frequency, $\alpha \to 0$. Once we pass through the cut-off frequency the proportion of scattered power transmitted into the ice sheet vanishes. However T, which is now the coefficient of the least-decaying mode, is finite and rapidly decreases, as shown in figure 9. The behaviour of $|T|$ above cut-off is of less interest and is omitted from the remaining figures.

The effect of adding compressive stress is shown in figure 11. For illustrative purposes we take $p = 110.5$ and $\theta = \pi/6$. At the higher frequencies either ϵ is large, or the transmission angle exceeds θ_c; either way the compressive stress has no effect. On decreasing the frequency, however, a regime is encountered in which $p\kappa^2\phi_z(x,0)$ becomes the largest term in the plate equation (cf. figure 2). Thus the ice sheet becomes relatively rigid and this leads to the high values of the reflection coefficient for $\omega \approx 0.6$ in figure 11. At very low frequencies, however, $\delta \sim \omega^{-2}$ and $\kappa \sim \omega^{-1}$, and so the boundary condition becomes

$$\left(1 - \frac{p\kappa^2}{\delta}\right)\phi_z(x,0) + \phi(x,0) \sim 0. \tag{8.1}$$

In contrast to the compression-free case, this is not the boundary condition for the free surface, but corresponds to a mass-loading boundary condition in which the role of the density difference between the fluid and the surface layer is played by compressive stress. Hence these stresses can have a significant effect upon the scattered fields, provided the angle of incidence of the incoming waves is larger than zero.

8.1. *Simple approximations*

The main complication in computing the Wiener–Hopf solution is in evaluating the product split, $\mathscr{K}(\xi) = \mathscr{K}_+(\xi)\mathscr{K}_-(\xi)$. Explicitly, we calculate the split functions using an integral:

$$\mathscr{K}_\pm(\xi) = -\mathrm{i}\sqrt{\epsilon}\,(\xi \pm \mathrm{i})^2\mathscr{R}_\pm(\xi)\frac{(\xi \pm \alpha)}{(\xi \pm \gamma)}, \tag{8.2}$$

where

$$\log \mathscr{R}_\pm(\xi) = \exp\left\{\pm\frac{1}{2\pi\mathrm{i}}\int_{-\infty\mp\mathrm{i}a}^{\infty\mp\mathrm{i}a}\frac{\log \mathscr{R}(\zeta)}{(\zeta - \xi)}\mathrm{d}\zeta\right\} \tag{8.3}$$

and

$$\mathscr{R}(\xi) = \frac{[\delta - (\epsilon\Gamma^4 - p\kappa^2 + \delta - 1)\Gamma\,\tanh\Gamma H](\xi^2 - \gamma^2)}{\epsilon(1 - \Gamma\,\tanh\Gamma H)(\xi^2 - \alpha^2)(\xi^2 + 1)^2}. \tag{8.4}$$

In applications of our scattering theory, repeated numerical evaluation of the exact solution may be necessary, and this can become numerically expensive due to the evaluation of the complex integrals in (8.3). In this section, we describe two ways in

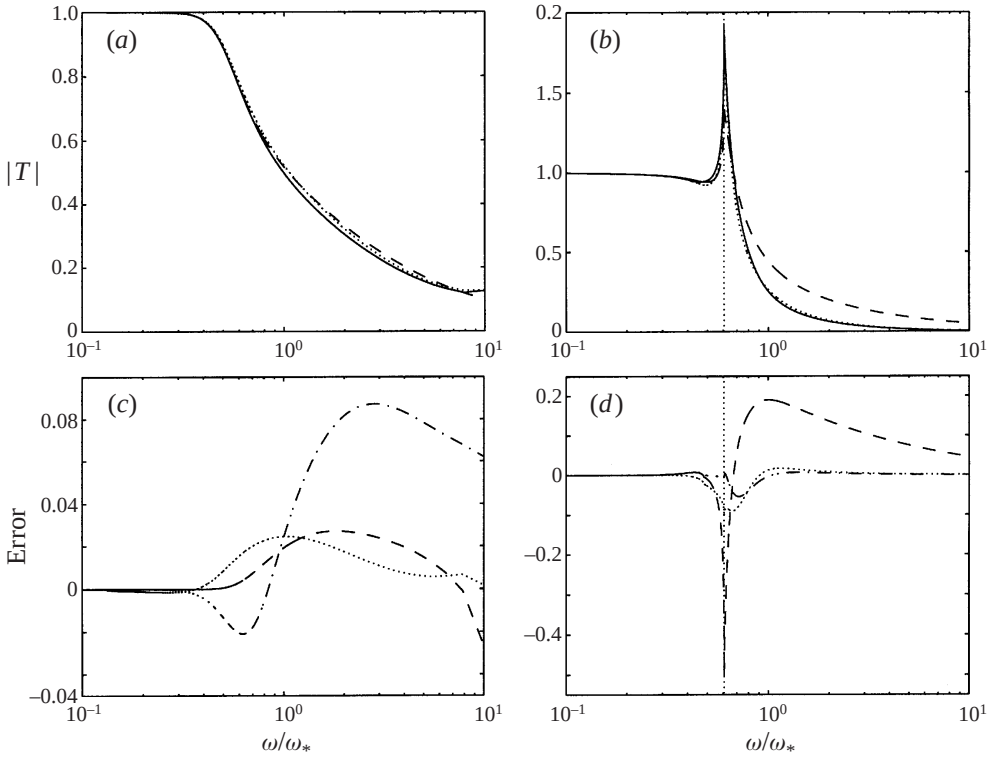

FIGURE 12. Transmission coefficients, $|T|$, for (*a*) $\theta = 0$ and (*b*) $\theta = \pi/3$. The exact solutions are shown by solid lines; the calculation using the the approximation (8.8) for $\mathscr{K}^1_+(\xi)$ is displayed as the dotted line and that using approximation (8.6) is shown as the dashed line. The errors in these approximations are shown in (*c*) and (*d*), together with that for the approximation $K^0_+(\xi)$; this is the dot-dashed line.

which we can avoid the evaluation of the integral in (8.3). This leads to two relatively simple approximations of the full solution.

The edge conditions amount to constraints upon various derivatives of the plate displacement at $x = 0^{\pm}$. A simpler approximation is furnished if, instead of satisfying the full edge conditions, we aim only for continuity of displacement across the edge. This amounts to neglecting $\mathscr{K}_+(\gamma)(A\gamma + B)$ in equation (7.6), and gives

$$|R| = \left|\frac{\alpha - \gamma}{\alpha + \gamma}\right|, \tag{8.5}$$

where α is the unapproximated travelling wavenumber in the ice-covered region. The power-flow relation then leads to

$$|T| = \frac{2}{(\alpha + \gamma)}\left[\frac{\alpha\delta\gamma\mathscr{D}'_{sea}(\gamma)}{\mathscr{D}'_{ice}(\alpha)\Gamma(\alpha)\tanh\Gamma(\alpha)H}\right]^{1/2}. \tag{8.6}$$

This approximation also corresponds to the parameter limit $\epsilon \ll \delta$, hence the accuracy declines as ω increases. None the less, the approximation has the attractive feature that it no longer requires the full factorization of $\mathscr{K}(\xi)$ and the solution of the simultaneous equations in (6.26) for A and B. As this approximation utilizes the exact dispersion relation, it incorporates the correct cut-off frequency.

Our second simplification arises from a direct approximation of the product split

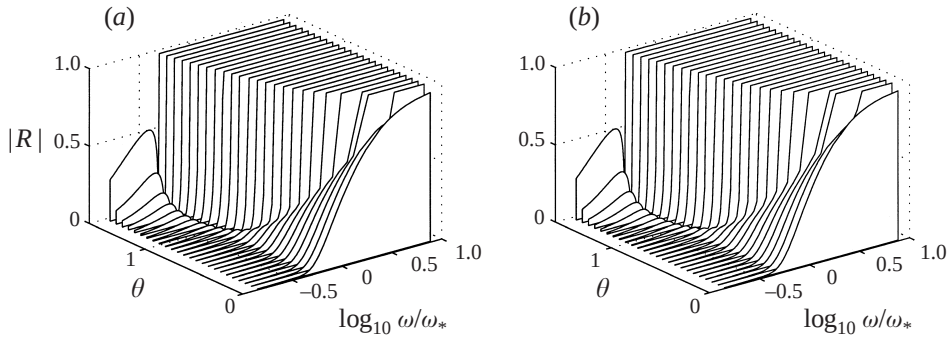

FIGURE 13. The reflection coefficient $|R|$ for infinite depth as a function of the angle of incidence θ of the incoming ocean waves and frequency: (*a*) the exact result and (*b*) the result evaluated using the approximate representation (8.7)–(8.8) for the product split in the analysis rather than the full exact factorization.

itself. In Appendix B we introduce an explicit, and reasonably accurate, approximation to $\mathscr{K}_+(\xi)$:

$$\mathscr{K}_+^{(0)}(\xi) \approx -\frac{\mathrm{i}\gamma}{\alpha|\xi_q|^2}\left|\frac{\mathscr{D}_{ice}(0)}{\mathscr{D}_{sea}(0)}\right|^{1/2}\frac{(\xi+\alpha)(\xi+\xi_q)(\xi-\xi_q^\star)}{(\xi+\gamma)}. \tag{8.7}$$

This formula involves the two real zeros, and quartet of complex zeros, of the ice-covered dispersion relation. Given these zeros of the dispersion relation, we continue on to solve equation (6.26) for A and B, and then construct T with $|R|$ evaluated from the power-flow relation.

The largest error introduced in using $\mathscr{K}_+^{(0)}$ arises from evaluating $\mathscr{K}_+(\gamma)$ (see Appendix B). However, we also have an exact formula for the magnitude of this quantity in (B 4). Hence we can improve the approximation on using the expression

$$\mathscr{K}_+^{(1)}(\gamma) \approx \left|\frac{(\alpha+\gamma)}{2\gamma(\alpha-\gamma)}\frac{(1-\mu^4\epsilon+p\kappa^2)}{\mathscr{D}'_{sea}(\gamma)}\right|^{1/2}\exp\{\mathrm{i}\arg[\mathscr{K}_+^{(0)}(\gamma)]\} \tag{8.8}$$

(so we only approximate the phase of $\mathscr{K}_+(\gamma)$).

In figure 12 we show transmission coefficients derived using the approximations. A more systematic comparison of our most accurate approximation (8.7)–(8.8) with the full numerical solution is shown in figure 13. The figure shows the comparison for infinite depth, but a similar level of accuracy is obtained for other fluid depths. Moreover, the approximation exactly locates the cut-off frequency and reduces to the shallow-water solution at small H.

9. Concluding remarks

In this study, we have provided an explicit solution of the scattering problem for ocean waves incident on ice-covered sea. We have deliberately kept the model for the ice sheet as general as possible, thus demonstrating that the analytical methods we employ are widely applicable. If, at some later date, it emerges that other plate models are more realistic, the analysis should follow that described here in a straightforward fashion.

Non-dimensionalization brings out the physical effects that are of primary importance; this shows that a thick-plate model is not required, without any computation whatsoever. We described detailed calculations based upon the thin-plate model; a

Floating dock: all depths	$\lvert R\rvert = 1$ $\lvert T\rvert = 0$
Mass loading: all depths $\delta > 1$ $\epsilon = 0$	$\lvert R\rvert = \left\lvert \dfrac{\alpha-\gamma}{\alpha+\gamma}\right\rvert$ $\lvert T\rvert = \dfrac{2\gamma}{(\alpha+\gamma)}\left[(\delta-1)\dfrac{\alpha\mathscr{D}'_{sea}(\gamma)}{\gamma\mathscr{D}'_{ice}(\alpha)}\right]^{1/2}$
Elastic plate: shallow water $\xi_0 = \alpha$, $\xi_1 = \xi_q$, $\xi_2 = -\xi_q^*$ $A_0 = T$ A_1 and A_2 complex constants.	$1 + R = T + A_1 + A_2,$ $\gamma(1-R) = \alpha T + \xi_1 A_1 + \xi_2 A_2$ $\sum_{i=0}^{2}(\xi_i^2 + \kappa^2)A_i(\xi_i^2 + \nu\kappa^2) = 0,$ $\sum_{i=0}^{2}\xi_i(\xi_i^2 + \kappa^2)A_i[\xi_i^2 + (2-\nu)\kappa^2] = 0$
Elastic plate: $\epsilon \ll \delta$, $\mathscr{D}_{ice}(\alpha) = 0$	$\lvert R\rvert = \left\lvert \dfrac{\alpha-\gamma}{\alpha+\gamma}\right\rvert$ $\lvert T\rvert = \dfrac{2}{(\alpha+\gamma)}\left[\dfrac{\alpha\delta\gamma\mathscr{D}'_{sea}(\gamma)}{\Gamma(\alpha)\tanh\Gamma(\alpha)H\mathscr{D}'_{ice}(\alpha)}\right]^{1/2}.$
Elastic plate: all depths A and B are solutions to (6.26)	$\lvert R\rvert = \left\lvert \dfrac{(\alpha-\gamma)}{(\alpha+\gamma)\Xi}\right\rvert \lvert[2\mathrm{i}\gamma\mathscr{K}_+(\gamma)(A\gamma + B) - \Xi]\rvert$
The split function, $\mathscr{K}_+(\xi)$, is determined numerically using (8.2)–(8.4) or approximately from (8.7)–(8.8).	$\lvert T\rvert^2 = \dfrac{\delta(\lvert R\rvert^2 - 1)\mathscr{D}'_{sea}(\gamma)}{\mathscr{D}_{ice}(\alpha)\Gamma(\alpha)\tanh\Gamma(\alpha)H}$

TABLE 4. The various limiting cases and the associated reflection and transmission coefficients. $\xi = \gamma$ and $\xi = \alpha$ denote the real (positive) solutions to the dispersion relations, $\mathscr{D}_{sea}(\xi) = 0$ and $\mathscr{D}_{ice}(\xi) = 0$, respectively. If α is not real, then all the incident power is reflected, thus $|R| = 1$; in the table we have given $|T|$ for frequencies below cut-off. ξ_q denotes the member of the dispersion relation, $\mathscr{D}_{ice}(\xi) = 0$, in the first quadrant. κ is the wavenumber in the direction of the ice edge.

particular advantage of having the explicit solution is that limiting cases and useful approximations emerge. A summary of these cases, together with the full solution is given in table 4; this contains known earlier results (the floating-dock, mass-loading and shallow-water limits) as well as our, all encompassing, elastic-plate results.

The solution we have found, together with the approximations described in § 8.1, provide a vital building block for a study of the fracture of shore-fast sea ice. In addition the full solution is a useful benchmark against which numerical studies can be compared. However, the solution is also useful in situations in which the ice sheet has a more complicated structure or geometry. In those applications, one can open asymptotic expansions with the Wiener–Hopf solution (such asymptotic expansions in water wave theory are described by Leppington 1992). For example, one can analyse scattering from finite ice floes (Meylan & Squire 1993, 1994, 1996) and inhomogeneous ice sheets. A notable application in the climatology of polar regions concerns how multiple scatterings affect the wave spectrum in the Marginal Ice Zone (Masson & LeBlond 1989).

The shallow-water limit provides a simpler route into analysing the ice sheet problem, without any of the technicalities of the Wiener–Hopf approach. Thus it provides a model wherein additional physical effects can be incorporated. In particular, we regard the shallow-water limit as the simplest setting in which to advance into a

more complete study of the process of fracture. Notably, this setting is a natural one for understanding the sporadic calving of icebergs from ice tongues.

Finally, it is worthwhile to note that this study, although focused upon scattering by ice sheets, is relevant for any physical situation involving the scattering of water (or any other fluid) waves by some floating flexible plate or membrane. Examples might include floating molten glass in an industrial process, or flexible floating platforms in the oil industry.

The financial support of an EPSRC Advanced Fellowship is gratefully acknowledged by R.V.C. We are grateful for the stimulating environment, and support, of the 1998 Geophysical Fluid Dynamics summer study program, Woods Hole Oceanographic Institution. N.J.B. was partially supported by the NSF Grant OCE-9616017, and thanks the ISI Foundation, Torino, for hospitality during part of this work. It is also a pleasure to thank Professor J. B. Keller for helpful conversations.

Appendix A. Transform formalities

In the main text we introduce the transforms $\Phi_{\pm}(\xi, z)$. There is a potential difficulty in defining these functions as the scattered wave amplitude does not necessarily decay as $x \to \pm\infty$. In that circumstance, $\Phi_{-}(\xi, z)$ only converges for $\mathrm{Im}\,(\xi) < 0$, and $\Phi_{+}(\xi, z)$ for $\mathrm{Im}\,(\xi) > 0$. That is, $\Phi_{-}(\xi, z)$ is analytic in the lower half-plane, and $\Phi_{+}(\xi, z)$ in the upper half-plane. With analytic continuation we may then define these functions over the whole plane and construct $\Phi(\xi, z) = \Phi_{-}(\xi, z) + \Phi_{+}(\xi, z)$. However, these analyticity properties alone do not provide sufficient information about $\Phi_{\pm}(\xi, z)$ in order to employ the Wiener–Hopf technique; more details of their analytic structure are needed. We obtain these details by briefly considering the dispersion relations in the open and ice-covered ocean. Similar considerations enable us to split the functions $\mathscr{K}_{\pm}(\xi)$ as desired.

In either the open ocean or the ice-covered sea, one can decompose any disturbance into normal modes. As described by Evans & Davies (and also Fox & Squire), these normal modes have characteristic wavenumbers which follow from the dispersion relations (2.17) and (5.4). For the open ocean there are two solutions for ξ that are located on the real axis, $\xi = \pm\gamma$, and an infinite number of solutions lying along the imaginary axis (see figure 3*a*). For ice-covered sea, there may again be two on the real axis, $\xi = \pm\alpha$. In addition, there is another host of solutions distributed along the imaginary axis, and a quartet of solutions with finite imaginary parts (figure 3*b*): $\xi = \pm\xi_q$ and $\pm\xi_q^*$. It is the solutions that lie upon the real axis that lead to potential difficulties.

The decomposition indicates that the solution for ϕ in the open ocean contains a part that does not decay as $x \to -\infty$ (the reflected wave), and a part decaying exponentially. The latter portion decays as fast as the mode with the least spatial decay rate in the superposition. This is the uppermost mode lying on the negative real axis in figure 3(*a*); the imaginary part of its eigenvalue is bounded from above, $\mathrm{Im}\,(\xi_{sea}) < -a$, for some positive constant a. By introducing the decomposition into the integral transform, we therefore see that $\Phi_{-}(\xi, z)$ must have a pole at $\xi = \gamma$, but is otherwise analytic in a strip, $\mathrm{Im}\,(\xi) < a$.

Similarly, the solution for ϕ in $x > 0$ contains the transmitted wave (if it exists) and a host of exponentially decaying contributions. Once again, the latter decay at least as fast as the modes in the superposition with smallest spatial decay rate. These modes are now in the upper half-plane and are either part of the quartet, $\pm\xi_q$, or the

lowest mode on the positive imaginary axis (see figure 3*b*). The eigenvalues of these modes can be bounded from below, $\mathrm{Im}\,(\xi_{ice}) > b$, for another positive constant, b. Thus $\Phi_+(\xi, z)$ is analytic in the strip, $\mathrm{Im}\,(\xi) > -b$, save for a pole at $\xi = -\alpha$.

In other words, we have two different regions in which the transforms, $\Phi_\pm(\xi, z)$, are analytic: $\Phi_-(\xi, z)$ is analytic over the region S_- and $\Phi_+(\xi, z)$ is analytic over S_+. Explicitly, we define S_- to be the strip $\mathrm{Im}\,(\xi) < a$, but with a piece cut out to remove the point $\xi = \gamma$, and S_+ as the strip $-b < \mathrm{Im}\,(\xi)$, with a section removed to avoid the point $\xi = -\alpha$.

A further technical detail arises when we split $\mathscr{K}(\xi)$. The split functions $\mathscr{K}_\pm(\xi)$ must be defined to be analytic and non-zero over the regions $S_\pm$. However, $\mathscr{K}(\xi)$ has zeros at all the roots of the ice-covered ocean dispersion relation, and poles at all the points in the open-ocean spectrum. This means that we need to also extract two further pieces from the strips in order to remove problems at $\xi = -\gamma$ and $\xi = \alpha$. To achieve this, we cut out a piece from S_- to remove $\xi = -\gamma$. Then we cut out another part of S_+ to remove the second problematic point at $\xi = \alpha$. Moreover, we need to modify the definition of a and b so that these constants bound both spectra. In particular, because each spectrum is symmetrical about the real axis, this means we must take both a and b to be less than the nearest eigenvalue to the real axis of either spectrum. In other words, we define $a = b$ as in figure 3, and the strips, $S_\pm$, as shown in figure 8.

With this definition of the two regions, $S_\pm$, we may define $\Phi_\pm(\xi, z)$ and $\mathscr{K}_\pm(\xi)$ with the desired analyticity and non-zero properties. Analyticity over the regions $S_\pm$ gives the proper definition of the meaning of the $\pm$ subscript. Furthermore, the two regions overlap in a cut strip parallel to the real axis, and this allows us to proceed with the Wiener–Hopf solution.

Given the form of the transforms, $\Phi_\pm(\xi, z)$, we may define the inverse

$$\frac{1}{2\pi}\int_{C_+} \Phi_+(\xi, y)\mathrm{e}^{-\mathrm{i}\xi x}\mathrm{d}\xi = \begin{cases} \phi(x, y) & \text{if } x < 0 \\ 0 & \text{if } x > 0 \end{cases} \tag{A 1}$$

and

$$\frac{1}{2\pi}\int_{C_-} \Phi_-(\xi, y)\mathrm{e}^{-\mathrm{i}\xi x}\mathrm{d}\xi = \begin{cases} 0 & \text{if } x < 0 \\ \phi(x, y) & \text{if } x > 0, \end{cases} \tag{A 2}$$

where $C_\pm$ run along the real axis, with C_- indented below $\xi = \gamma$ and α, and C_+ indented above $\xi = -\alpha$ and $-\gamma$. Both (A 1) and (A 2) are equivalent, for all x, to

$$\phi(x, z) = \frac{1}{2\pi}\int_C \Phi(\xi, z)\mathrm{e}^{-\mathrm{i}\xi x}\mathrm{d}\xi, \tag{A 3}$$

where C runs along the real axis, but indented below $\xi = \gamma$ and α, and above $\xi = -\alpha$ and $-\gamma$.

When the dissipative terms in the plate equation do not vanish (they were implicitly ignored in the discussion above), then the characteristic wavenumbers, $\pm\alpha$, are displaced off the real axis. In particular, $\xi = -\alpha$ is pushed into the upper half-plane. This means that the transform $\Phi_+(\xi, z)$ will automatically be analytic in an overlapping strip surrounding the real axis. But problems remain due to the non-decaying reflected wave. In this case we need not explicitly consider the points $\xi = \pm\alpha$, and we define $S_\pm$ with sections removed to extract only $\xi = \pm\gamma$. If the reflected wave were also decaying we could, in fact, also ignore these latter points and take $S_\pm$ to contain the entire upper and lower half-planes, respectively, with a region of overlap being a strip containing the real axis. The formal Wiener–Hopf solution and the definition

of the integration contours of the inverse transform are then much more straightforward. For such reasons, one conventional method for dealing with the non-dissipative problem is to introduce a small dissipation term into the problem at the outset, and then later limit this to zero; but this diversion is unnecessary.

Appendix B. The Wiener–Hopf splits

In the text, the function $\mathscr{K}(\xi)$ has to be split into a product of functions that are analytic and non-zero in the $\pm$-regions, $S_\pm$: $\mathscr{K}(\xi) = \mathscr{K}_+(\xi)\mathscr{K}_-(\xi)$. To achieve this factorization it is first convenient to extract explicitly any poles or zeros in $\mathscr{K}(\xi)$ that lie on the real axis (namely those at $\xi = \pm\gamma$ and $\xi = \pm\alpha$, respectively). We then define

$$\mathscr{R}(\xi) = \frac{\mathscr{D}_{ice}(\xi)}{\mathscr{D}_{sea}(\xi)} \frac{(\xi^2 - \gamma^2)}{(\xi^2 - \alpha^2)} \frac{1}{N(\xi)},$$

where the function $N(\xi)$ is chosen so that $\mathscr{R}(\xi) \to 1$ as $|\xi| \to \infty$ and to be analytic and non-zero over $-a < \mathrm{Im}\,(\xi) < a$, where the constant a is given meaning in Appendix A and drawn in figure 3.

Our aim is to split $\mathscr{R}(\xi)$ into the product $\mathscr{R}_+(\xi)\mathscr{R}_-(\xi)$. Because we have extracted all poles and zeros from $\mathscr{R}(\xi)$ for $-a < \mathrm{Im}\,(\xi) < a$, it follows that $\mathscr{R}(\xi)$ is analytic over this strip of the complex plane. Hence, if we define

$$\log \mathscr{R}_-(\xi) = -\frac{1}{2\pi \mathrm{i}} \int_{-\infty+\mathrm{i}a}^{\infty+\mathrm{i}a} \frac{\log \mathscr{R}(\zeta)}{(\zeta - \xi)} \mathrm{d}\zeta \text{ and } \log \mathscr{R}_+(\xi) = \frac{1}{2\pi \mathrm{i}} \int_{-\infty-\mathrm{i}a}^{\infty-\mathrm{i}a} \frac{\log \mathscr{R}(\zeta)}{(\zeta - \xi)} \mathrm{d}\zeta, \tag{B 1}$$

for $-a < \mathrm{Im}(\xi) < a$, then $\log \mathscr{R}_+ + \log \mathscr{R}_- = \log \mathscr{R}$ by Cauchy's Residue Theorem (and because $\mathscr{R} \to 1$ and $|\xi| \to \infty$). But, the properties of the Cauchy integrals in (B 1) imply that $\log \mathscr{R}_+(\xi)$ is analytic for $\mathrm{Im}\,(\xi) > -a$, and that $\mathscr{R}_-(\xi)$ is analytic for $\mathrm{Im}\,(\xi) < a$. In other words, the integrals are $\pm$ functions and suffice to define the splitting. Note that the logarithm ensures that these functions are also non-zero.

Equation (B 1) contains two important formulae; the numerical construction of the Wiener–Hopf solution centres around finding the product split. These integrals can, in fact, be computed using relatively simple quadratures (in practice we replace the limits by $\pm L + \mathrm{i}a$ and $\pm L - \mathrm{i}a$; the integrals converge rapidly as $L \to \infty$).

For the thin-plate model with compression, we define $\mathscr{R}(\xi)$ as

$$\mathscr{R}(\xi) = \left\{ \frac{\Gamma(\xi)\tanh\Gamma(\xi)H[\epsilon\Gamma^4(\xi) - p\kappa^2 + \delta - 1] - \delta}{\Gamma(\xi)\tanh\Gamma(\xi)H - 1} \right\} \frac{(\xi^2 - \gamma^2)}{(\xi^2 - \alpha^2)\epsilon(\xi^2 + 1)^2} \tag{B 2}$$

(so $N = \epsilon(\xi^2 + 1)^2$). Given $\mathscr{R}_\pm(\xi)$, we then construct $\mathscr{K}_\pm(\xi)$ from

$$\mathscr{K}_+(\xi) = -\mathrm{i}\sqrt{\epsilon}\,(\xi + \mathrm{i})^2 \mathscr{R}_+(\xi) \frac{(\xi + \alpha)}{(\xi + \gamma)} \text{ and } \mathscr{K}_-(\xi) = -\mathrm{i}\sqrt{\epsilon}\,(\xi - \mathrm{i})^2 \mathscr{R}_-(\xi) \frac{(\xi - \alpha)}{(\xi - \gamma)}. \tag{B 3}$$

The choice of $N(\xi)$ is not unique; here it is chosen to enforce the correct behaviour at infinity, and to introduce no poles within the strip $-a < \mathrm{Im}\,(\xi) < a$ (other fourth-order polynomials would also suffice, with consequent changes in (B 3)). Also, we can extract the formulae

$$|\mathscr{K}_+(\gamma)|^2 = \left| \frac{(\alpha + \gamma)}{2\gamma(\alpha - \gamma)} \frac{(1 - \mu^4\epsilon + p\kappa^2)}{\mathscr{D}'_{sea}(\gamma)} \right| \tag{B 4}$$

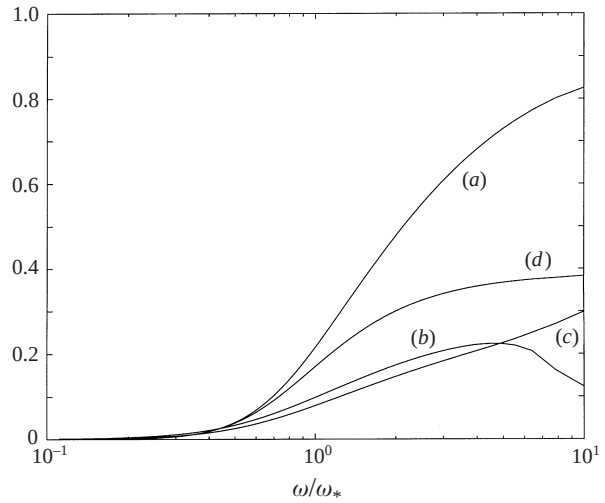

FIGURE 14. The approximate split (B 6) versus frequency for infinite depth, normal incidence, $h = 1.5$ m. The curve labelled (*a*) shows $|\mathscr{K}_+(\gamma) - \mathscr{K}_+^{(0)}(\gamma)|/|\mathscr{K}_+(\gamma)|$, (*b*) and (*c*) show the same quantity, but with γ replaced by χ_1 and χ_2 respectively. The curve labelled (*d*) shows $|\mathscr{K}_+(\gamma) - \mathscr{K}_+^{(1)}(\gamma)|/|\mathscr{K}_+(\gamma)|$.

and

$$|\mathscr{K}_+(\alpha)|^2 = \left| \frac{\mathscr{D}'_{ice}(\alpha)}{\mathscr{D}_{sea}(\alpha)} \frac{2\alpha(\alpha-\gamma)}{(\alpha+\gamma)} \right|, \tag{B 5}$$

which are used to simplify many of the results in the text. These relations follow by noticing that $\mathscr{R}(\xi)$ is even in ξ, real and positive for ξ real, and that $\mathscr{R}_+(\xi) = \mathscr{R}_-(-\xi)$; thus for ξ real, $|\mathscr{R}_+(\xi)|^2 = |\mathscr{R}(\xi)|$.

The scattering problem we solve in this paper is an important building block in more involved theories of ice fracture. Hence the full solution obtained in this paper will ultimately be used as a component part of more complicated, numerical work. Then the repeated evaluation of the complex quadrature (B 1) can become numerically expensive. Hence, it is useful to derive accurate approximations to the split functions. The most useful explicit approximation for $\mathscr{K}_+(\xi)$ is

$$\mathscr{K}_+^{(0)}(\xi) \approx -\frac{\mathrm{i}\gamma}{\alpha|\xi_q|^2} \left| \frac{\mathscr{D}_{ice}(0)}{\mathscr{D}_{sea}(0)} \right|^{1/2} \frac{(\xi+\alpha)(\xi+\xi_q)(\xi-\xi_q^\star)}{(\xi+\gamma)}. \tag{B 6}$$

This approximation allows us to find accurate solutions over a wide range of frequencies and fluid depths. This specific approximation is devised using the analytic structure associated with the quartet of zeros, $\pm\xi_q$ and $\pm\xi_q^*$, and the real zeros of the dispersion relations; this structure emerges naturally in our exact factorizations for infinite depth and shallow water. Thus one expects a similar structure to be important in the more general case. The ratio of the dispersion relations evaluated at the origin acts as a weighting factor ensuring accuracy is maintained at higher frequencies.

We plot the relative error of the approximation in figure 14 for $\xi = \gamma$, χ_1 and χ_2; these are the points at which we need to evaluate $\mathscr{K}_\pm(\xi)$ in the computation of the reflection and transmission coefficients. The worst approximation is for $\mathscr{K}_+^0(\gamma)$. However, in this case, we have an exact formula for the modulus of $|\mathscr{K}_+(\gamma)|$ in (B 4). Hence we can improve the approximation by using the exact magnitude of $\mathscr{K}_+(\gamma)$

and approximating only its phase. In fact, we may do this for all real ξ. Thus a more refined approximation is given by

$$\mathscr{K}_+^{(1)}(\xi) \approx -\frac{\mathrm{i}\gamma}{\alpha|\xi_q|^2}\left|\frac{\mathscr{D}_{ice}(0)}{\mathscr{D}_{sea}(0)}\right|^{1/2}\frac{|\mathscr{K}_+(\xi)|}{|\mathscr{K}_+^{(0)}(\xi)|}\frac{(\xi+\alpha)(\xi+\xi_q)(\xi-\xi_q^*)}{(\xi+\gamma)}. \tag{B 7}$$

The error in this approximation is also displayed in figure 14; the accuracy of $\mathscr{K}_+^{(1)}(\gamma)$ is markedly improved over $\mathscr{K}_+^{(0)}(\gamma)$. We compare the approximations with the full numerical solution in the main text (§ 8.1).

B.1. *Infinite depth*

For infinite depth the factorization (B 1) reduces to a simpler and more explicit form. To achieve this factorization, we first split the function (related to the numerator of $\mathscr{K}(\xi)$)

$$F(\xi) = \epsilon\Gamma^4(\xi) - p\kappa^2 + \delta - 1 - \frac{\delta}{\Gamma(\xi)}. \tag{B 8}$$

The denominator of $\mathscr{K}(\xi)$ is then dealt with in a similar, but simpler, manner. The analytic structure of $F(\xi)$ is the same as $\mathscr{D}_{ice}(\xi)$; that is, $F(\xi)$ has two real zeros at $\xi = \pm\alpha$, a quartet at $\xi = \pm\xi_q, \pm\xi_q^*$, and branch cuts along $[\mathrm{i}\kappa, \mathrm{i}\infty)$ and $[\mathrm{i}\kappa, -\mathrm{i}\infty)$ (the infinite sequence of zeros along the imaginary axis as shown in figure 3, is replaced, for infinite depth, by these branch cuts). The zeros of $F(\xi)$ are found numerically.

We next define

$$Q(\xi) = \frac{[\epsilon\Gamma^4(\xi) - p\kappa^2 + \delta - 1 - \delta/\Gamma(\xi)]\Gamma^2(\xi)}{\epsilon(\xi^2-\alpha^2)(\xi^2-\xi_q^2)(\xi^2-\xi_q^{*2})}, \tag{B 9}$$

which has no zeros in the cut plane and tends to unity for $|\xi| \to \infty$. For definiteness we treat $Q_-(\xi)$ in detail; because $Q(\xi)$ is an even function of ξ, then $Q_+(\xi) = Q_-(-\xi)$. The analytic structure of $Q(\xi)$ involves only branch cuts. Hence we evaluate $Q_-(\xi)$ by collapsing the integral around the cut in the upper half of the complex ξ-plane:

$$Q_-(\xi) = \exp\left\{-\frac{1}{\pi}\int_\kappa^\infty \tan^{-1}\left[\frac{\delta/\sqrt{q^2-\kappa^2}}{\epsilon(q^2-\kappa^2)^2 - p\kappa^2 + \delta - 1}\right]\frac{\mathrm{d}q}{q+\mathrm{i}\xi}\right\}, \tag{B 10}$$

where the branch of $\tan^{-1}\phi$ is chosen such that $0 \leqslant \tan^{-1}\phi \leqslant \pi$. Given $Q_\pm(\xi)$, we can explicitly identify $F_\pm(\xi)$.

B.2. *Shallow-water limit*

In the shallow-water limit,

$$\mathscr{K}(\xi) \sim -\frac{\epsilon\Gamma^6(\xi) + (\delta - 1 - p\kappa^2)\Gamma^2(\xi) - \delta/H}{\Gamma^2(\xi) - 1/H} = -\epsilon\frac{(\xi^2-\alpha^2)(\xi^2-\xi_q^2)(\xi^2-\xi_q^{\star 2})}{(\xi^2-\gamma^2)} \tag{B 11}$$

and the factorization is precisely of the form (B 6). The roots α and ξ_q are found explicitly in this limit from the roots of a cubic in $\Gamma^2(\xi)$: let

$$s_1^3 = \frac{\delta}{2H\epsilon}\left[\sqrt{\frac{4\delta H^2}{27\epsilon}\left(1 - \frac{(1+p\kappa^2)}{\delta}\right)^3 + 1} + 1\right] \tag{B 12}$$

and

$$s_2^3 = \frac{\delta}{2H\epsilon}\left[\sqrt{\frac{4\delta H^2}{27\epsilon}\left(1-\frac{(1+p\kappa^2)}{\delta}\right)^3+1}-1\right]. \tag{B 13}$$

Then $\Gamma^2(\alpha) = (s_1 - s_2)$ and $\Gamma^2(\xi_q) = s_1 e^{2\pi i/3} - s_2 e^{-2\pi i/3}$. The branch of the square root is chosen such that ξ_q is in the first quadrant.

The shallow-water results are also deduced by setting

$$\psi(x) = \begin{cases} R\exp(-i\gamma x) & \text{for } x < 0 \\ T\exp(i\alpha x) + A_1\exp(i\xi_q x) + A_2\exp(-i\xi_q^* x) & \text{for } x > 0. \end{cases} \tag{B 14}$$

(Evidently, in this limit the zeros of the ice-covered ocean dispersion function that lie on the imaginary axis recede to $\pm i\infty$.) Then, the continuity of ϕ and ϕ_z across $x = z = 0$ requires

$$1 + R = T + A_1 + A_2, \quad \gamma(1-R) = \alpha T + \xi_q A_1 - \xi_q^* A_2. \tag{B 15}$$

The edge conditions can then be written in the form

$$\sum_{i=0}^{2}(\xi_i^2+\kappa^2)A_i(\xi_i^2+\nu\kappa^2) = 0 \quad \text{and} \quad \sum_{i=0}^{2}\xi_i(\xi_i^2+\kappa^2)A_i[\xi_i^2+(2-\nu)\kappa^2] = 0, \tag{B 16}$$

where $T = A_0$ and $\alpha = \xi_0$, $\xi_1 = \xi_q$ and $\xi_2 = -\xi_q^*$. Hence we reduce the problem to an algebraic system. These equations are easily solved to furnish R and T.

REFERENCES

Bates, H. F. & Shapiro, L. H. 1980 Long-period gravity waves in ice covered sea. *J. Geophys. Res.* **85**, 1095–1100.

Craster, R. V. 1998 Scattering by cracks beneath fluid–solid interfaces. *J. Sound Vib.* **209**, 343–372.

Crighton, D. G. 1988 The 1988 Rayleigh medal lecture: fluid loading – the interaction between sound and vibration. *J. Sound Vib.* **133**, 1–27.

Evans, D. V. & Davies, T. V. 1968 Wave–ice interaction. *Stevens Inst. of Technology: Rep.* 1313.

Fox, C. & Squire, V. A. 1990 Reflection and transmission characteristics at the edge of shore fast sea ice. *J. Geophys. Res.* **95**, 11629–11639.

Fox, C. & Squire, V. A. 1991 Coupling between the ocean and an ice shelf. *Ann. Glaciol.* **15**, 101–108.

Fox, C. & Squire, V. A. 1992 On ice-coupled waves: a comparison of data and theory. In *Advances in Ice Technology*, *Proc. 2nd Int Conf. in Ice Tech.*, pp. 269–280. Boston.

Fox, C. & Squire, V. A. 1994 On the oblique relexion and transmission of ocean waves at shore fast ice. *Phil. Trans. R. Soc. Lond.* A **347**, 185–218.

Greenhill, A. G. 1887 Wave motion in hydrodynamics. *Am. J. Maths* **9**, 62–112.

Heins, A. E. 1948 Water waves over a channel of finite depth with a dock. *Am. J. Maths* **70**, 730–748.

Holdsworth, G. 1969 Flexure of a floating ice tongue. *J. Glaciol.* **8**, 385–397.

Holdsworth, G. & Glynn, J. E. 1981 A mechanism for the formation of large icebergs. *J. Geophys. Res.* **86**, 3210–3222.

Hunkins, K. 1962 Waves on the arctic ocean. *J. Geophys. Res.* **67**, 2477–2489.

Junger, M. C. & Feit, D. 1986 *Sound, Structures and Their Interaction*, 2nd Edn. Acoustical Society of America.

Keller, J. B. 1998 Gravity waves on ice-covered water. *J. Geophys. Res.* **103**, 7663–7669.

Keller, J. B. & Goldstein, E. 1953 Water wave reflection due to surface tension and floating ice. *Trans. Am. Geophys. Union* **34**, 43–45.

Keller, J. B. & Weitz, M. 1953 Reflection and transmission coefficients for waves entering or leaving an icefield. *Commun. Pure Appl. Maths* **6**, 415–417.

Kriegsmann, G. 1999 The flanged waveguide antenna: discrete reciprocity and conservation. *Wave Motion* **29**, 81–95.

Leppington, F. G. 1992 Matched asymptotic methods in surface wave theory. In *Wave asymptotics* (ed. P. A. Martin & G. R. Wickham), pp. 69–85. Cambridge University Press.

Lighthill, M. J. 1978 *Waves in Fluids*. Cambridge University Press.

Liu, A. K., Holt, B. & Vachon, P. W. 1991 Wave propagation in the marginal ice zone: model predictions and comparisons with buoy and SAR data. *J. Geophys. Res.* **96**, 4605–4621.

Liu, A. K. & Mollo-Christensen, E. 1988 Wave propagation in a solid ice pack. *J. Phys. Oceanogr.* **18**, 1702–1712.

Martin, S. & Kauffman, P. 1981 A field and laboratory study of wave damping by grease ice. *J. Glaciol.* **27**, 283–313.

Masson, D. & LeBlond, P. H. 1989 Spectral evolution of wind-generated surface gravity waves in a dispersed ice field. *J. Fluid Mech.* **202**, 43–81.

Meylan, M. H. & Squire, V. A. 1993 Finite-floe wave reflection and transmission coefficients from a semi-infinite model. *J. Geophys. Res.* **98**, 12537–12542.

Meylan, M. H. & Squire, V. A. 1994 The response of ice floes to ocean waves. *J. Geophys. Res.* **99**, 891–900.

Meylan, M. H. & Squire, V. A. 1996 Response of a circular ice floe to ocean waves. *J. Geophys. Res.* **101**, 8869–8884.

Mindlin, R. D. 1951 Influence of rotary inertia and shear on flexural motion of isotropic elastic plates. *Trans. ASME: J. Appl. Mech.* **18**, 31–38.

Mittra, R. & Lee, S. W. 1971 *Analytical Techniques in the Theory of Guided Waves*. Macmillan.

Newyear, K. & Martin, S. 1997 A comparison of theory and laboratory measurements of wave propagation and attenuation in grease ice. *J. Geophys. Res.* **102**, 25091–25099.

Noble, B. 1958 *Methods Based on the Wiener-Hopf Technique*. Pergamon.

Peters, A. S. 1950 The effect of a floating mat on water waves. *Commun. Pure Appl. Maths* **3**, 319–354.

Robin, G. de Q. 1963 Wave propagation through fields of pack ice. *Phil. Trans. R. Soc. Lond.* A **255**, 313–339.

Robinson, N. J. & Palmer, S. C. 1990 A modal analysis of a rectangular plate floating on an incompressible liquid. *J. Sound Vib.* **42**, 453–460.

Shapiro, A. & Simpson, L. S. 1953 The effect of a broken ice field on water waves. *Trans. Am. Geophys. Union* **34**, 36–42.

Squire, V. A. 1984 A theoretical, laboratory and field study of ice–coupled waves. *J. Geophys. Res.* **89**, 8069–8079.

Squire, V. A., Dugan, J. P., Wadhams, P., Rottier, P. J. & Liu, A. K. 1995 Of ocean waves and sea–ice. *Ann. Rev. Fluid Mech.* **27**, 115–168.

Squire, V. A., Robinson, W. H., Meylan, M. & Haskell, T. G. 1994 Observations of flexural waves on the Erebus-ice-tongue, McMurdo-sound, Antarctica, and nearby sea–ice. *J. Glaciol.* **40**, 377–385.

Timoshenko, S. & Woinowsky-Krieger, S. 1959 *Theory of Plates and Shells*. McGraw-Hill.

Ungar, E. E. 1988 Damping of panels. In *Noise and Vibration Control* (ed. B. L. E.), chap. 14. Institute of Noise Control Engineering.

Wadhams, P. 1973*a* Attenuation of swell by sea ice. *J. Geophys. Res.* **78**, 3552–3565.

Wadhams, P. 1973*b* The effect of a sea ice cover on ocean surface waves. University of Cambridge, PhD Thesis.

Wadhams, P. 1986 The seasonal ice zone. In *The Geophysics of Sea Ice* (ed. N. Untersteiner), chap. 14. Plenum.

Wadhams, P. 1995 Arctic sea ice extent and thickness. *Phil. Trans. R. Soc. Lond.* A **352**, 301–319.

Wadhams, P. & Holt, B. 1991 Waves in frazil and pancake ice and their detection in Seasat synthetic aperture radar imagery. *J. Geophys. Res.* **96**, 8835–8852.

Weitz, M. & Keller, J. B. 1950 Reflection of water waves from floating ice in water of finite depth. *Commun. Pure Appl. Maths* **3**, 305–318.